ELSEVIER

Polymer 40 (1999) 3119–3145

polymer

Structural hierarchy developed in co-injection molded polystyrene/polypropylene parts

M. Kadota[a], M. Cakmak[a,*], H. Hamada[b]

[a]*Polymer Engineering Institute, University of Akron, Akron, OH 44325-0301, USA*
[b]*Kyoto Institute of Technology, Department of Polymer Science and Engineering, Kyoto, Japan*

Received 13 March 1998; revised 5 June 1998; accepted 10 June 1998

Abstract

In this paper, the structural gradients developed in co-injection molded polypropylene/polystyrene parts were investigated as a function of process history and injection sequence. For this purpose, a series of parts with PP skin/PS core, PS skin/PP core, and PP skin/PP core were prepared under selected mold temperatures and injection speeds and detailed structural analyses were performed using a series of structural analysis techniques. The optical microscopy, microbeam-WAXS and birefringence techniques revealed that crystalline orientation levels in PP are high when it is injected first to form the outer (skin) layer of the part. On going from the mold surface to the polystyrene surface the orientation level decreases slightly but remains high even at the PS/PP interface that is located at the interior of the part. This result is mainly caused by the additional deformation that the PP experiences as a result of secondary shearing by the polystyrene injection that occurs a short time delay after the primary injection. When PP is injected as a core layer, the orientation levels in PP were found to be low and mainly concentrated near the PP/PS interface. This low level of orientation is as a result of slower cooling that causes the relaxation of the chain orientation developed during the flow prior to the crystallization. In all polystyrene skin samples, the birefringence between the two skins was found to be the highest at the intermediate distances. When the injection speed of the core polypropylene is increased, this peak position shifts towards the mold surface as a result of shear heating. The use of low injection speeds in the core layer injection was found to distribute this layer more uniformly along the flow path. This is attributed to the attainment of increased levels of viscosity for the first injected layers during the course of injection of core layers at slower speeds.

Keywords: Co-injection moulding; Polypropylene; Structure development

1. Introduction

The co-injection molding process was first developed by ICI in the UK in early 1970s and has become one of the major production methods in recent years [1]. This process is also known by other names such as sandwich injection molding, or multi-injection molding in the case where two or more materials are involved. This process has found utility in the recycling area where scrap material can be injected as the core layer while a high quality virgin material forms the exterior regions of the parts [2,3].

In simultaneous co-injection molding the two materials in two different barrels are injected into a mold at the same time to form parts with skin–core morphology. On the other hand, the sequential injection molding is conducted in such a way that one material which will form a skin part is injected first then the second material forms the core regions.

Some of the basic ideas used to explain this process come from the studies of stratified two-phase flow of polymer melts through dies [4–10]. Nagano [4] and Southern and Ballman [6] have shown that in stratified flow through cylindrical dies low viscosity melt gradually encapsulates a higher viscosity melt. This has been verified more recently by several researchers [7,8,10,11]. Young et al. [12] have conducted extensive research on the sandwich injection molding process. It was emphasized that the viscosity ratio of the second injected material to that of the first injected material plays an important role in the formation of the interfacial shape. If the ratio is too large, the material injected in the second stage does not penetrate sufficiently deep into the first melt resulting in a part with poor skin thickness uniformity and the second polymer remaining only near the gate. When the viscosity of the second material is too low (the ratio is too small), the second melt tends

* Corresponding author. Tel.: +1-330-972-6865; Fax: +1-330-258-2339; E-mail: cakmak@uakron.edu

0032-3861/99/$ - see front matter
PII: S0032-3861(98)00472-8

to completely penetrate through the first injected material resulting in ''burst through''. Only in the intermediate viscosity ratio, can one obtain both encapsulation and uniform thickness [13,14].

It is also possible to make such a sandwich mold by simultaneously injecting two materials. Menges and his coworkers [15] have considered a similar problem in which a melt injected into a mold is separated into two streams and a foaming agent is injected into the annular system. White and Lee [10] conducted an experimental study of an annulus–core configuration of injection molding using an Instron capillary rheometer, which simulates the simultaneous injection molding. They reached a conclusion similar to the sequential injection molding. Since at the interface in annual flow, the shear stresses σ_{12} are equal in each phase, the equation proposed below explains the channeling of the lower viscosity core:

$$\mu_A \frac{\partial u_A}{\partial r}\bigg|\text{annulus} = \mu_B \frac{\partial u_B}{\partial r}\bigg|\text{core}$$

A high viscosity core will possess a lower interface velocity gradient and an average velocity not much greater than the lower viscosity annular ring. On the other hand, the lower viscosity core will possess a large interfacial velocity gradient and a considerably higher average velocity than the higher viscosity annulus.

Although the structural development in injection molded straight injection molded polypropylene [16–24] and atactic [25] and syndiotactic polystyrene [26] has been extensively investigated, their behavior in the co-injection molding process has not been studied.

In this study, our focus is on the development of the structure gradients in co-injection molded parts of varying processing history. By using immiscible polypropylene and polystyrene as the two injection materials, it is ensured that there is a distinct interface between the polymers. This will allow us to observe the effect of molding parameters and injection sequence on the skin and core materials. The tools used to identify and quantify the structural parameters are polarized light microscopy, birefringence, microbeam-WAXS methods and pole wide angle X-ray. The latter technique is particularly suited for investigating the sharp structural gradients that are observed in injection molded parts [27–29].

2. Experimental procedures

2.1. Materials

The materials used in this experiment were E200 (Tonen Chemical Co., Ltd.) non-nucleated polypropylene and Styron 666 (Asahi Chemical Co., Ltd.) polystyrene. The weight average molecular weight of polypropylene (M_w) was 450 000 and MFR (230°C, 2160 g) 0.5. The weight average molecular weight of polystyrene (M_w) was 240 000. The viscosity of polypropylene and polystyrene used in this experiment was measured at three different temperatures, 190°C, 210°C, and 230°C, using an Instron capillary rheometer. The data were corrected for end pressure losses.

2.2. Sample preparation

The samples were prepared with the 80 ton Toyokikai-kinnzoku Model # TP–80G$_{2H1}$ co-injection molding machine, at a series of mold temperatures and injection

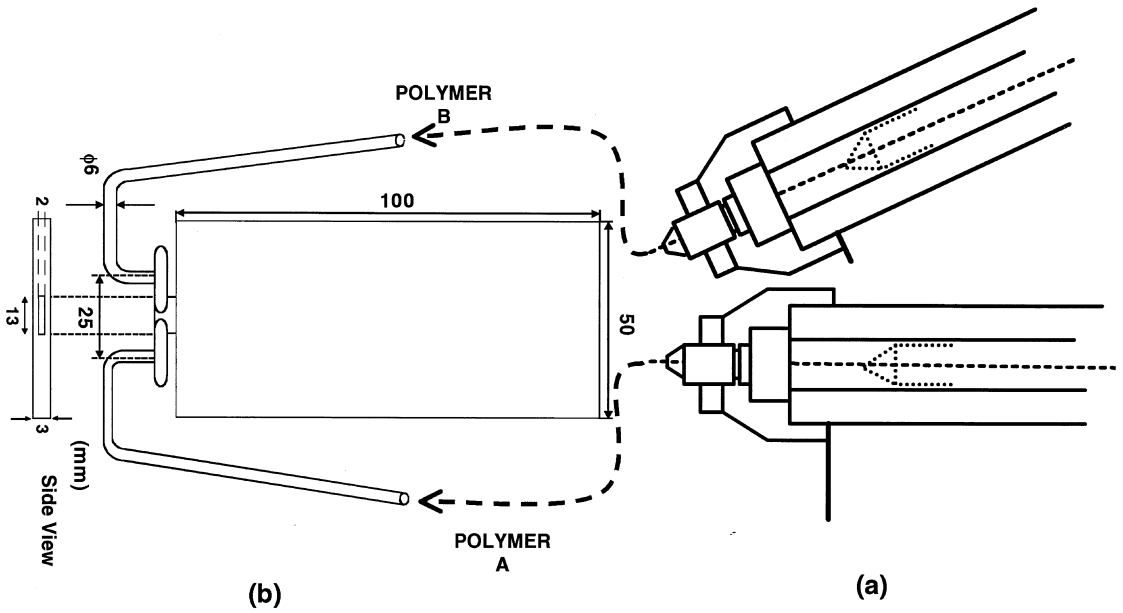

Fig. 1. (a) Co-injection molding nozzle section. (b) Cavity geometry.

speeds. This co-injection molding machine is equipped with an 80 ton clamping unit and with two 38 cm^3 injection units oriented at an angle of 25° to each other in order to shorten the sprue distance. The nozzle section of this machine is schematically shown in Fig. 1(a). The actions of the two injection units are independently controllable. This allows the adjustment of the time lag between the onsets of the two injections.

This machine was operated in sequential mode: one material that would form a skin part was injected 1 s prior to the second material that would later form the core of the part. The injection time lag is set so that the core material reaches the gate at the time of the completion of the injection of skin material. The holding pressure is applied only by the injection unit of the core material after the completion of the cavity fill. The cavity design used in this work is shown Fig. 1(b). In this design, the two runners with 6 mm circular cross-sections pass the melt from the sprue to the gate. A rectangular gate with 13 mm × 2 mm dimensions forms the center portion of one end of the rectangular cavity with 100 mm × 50 mm × 3 mm dimensions.

All the processing conditions are indicated in Table 1. All samples were produced with 230°C melt temperature and 40 s holding time. As indicated in Table 1, the effect of injection speed and mold temperature on the structure of the parts can be studied. Three samples were made for each condition.

2.3. Sample cutting procedure

All specimens were carefully diced into ten small pieces with a Leco Varicut VC-50 diamond saw. Three cutting procedures were used to section the samples as shown in Fig. 2. Procedure A consisted of cutting sections perpendicular to the flow direction in the TD–ND plane.

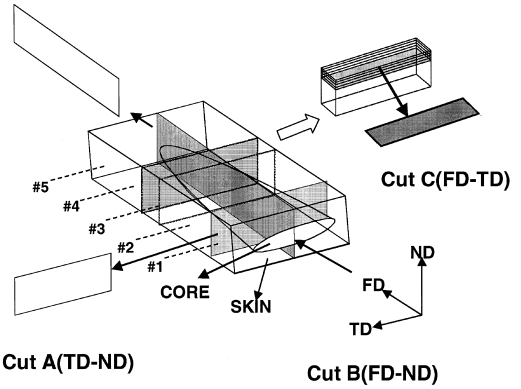

Fig. 2. Sample cutting procedures A, B and C.

In procedure B the samples were sectioned parallel to the flow direction in the FD–ND plane, along the center of the sample. Finally, procedure C consisted of cutting sections from skin to core, parallel to the flow direction in the FD–TD plane.

2.4. Optical microscopy

2.4.1. Micrographs

Samples of 10 μm in thickness were cut using a Reichert–Jung 2050 microtome. They were then sandwiched between two glass slides and placed on the microscope stage and oriented with their long axes at 45° to polarization directions of crossed polarizers. The transmission optical photomicrographs were taken through a Leitz Laborlux 12 POL S microscope using a Sony CCD camera as well as a Nikon 8008S camera.

2.4.2. Birefringence measurement of B-cut samples

The birefringence (Δn_{13}) (1 = flow direction, 3 = thickness direction) was measured for samples with skin

Table 1
Molding conditions

Sample number	PS injection speed ($cm^3\,s^{-1}$)	PP injection speed ($cm^3\,s^{-1}$)	Mold temperature (°C)	Ratio of charge (Volume PP/PS)	Holding pressure (kgf)
10	13.68	5.47	50	35/34	100 (10 s)
11	13.68	16.41	50	35/34	100 (10 s)
12	13.68	27.35	50	35/34	100 (10 s)
13	13.68	5.47	70	35/34	100 (10 s)
14	13.68	16.41	70	35/34	100 (10 s)
15	13.68	27.35	70	35/34	100 (10 s)
16	13.68	5.47	90	35/34	100 (10 s)
17	13.68	16.41	90	35/34	100 (10 s)
18	13.68	27.35	90	35/34	100 (10 s)
Specimens from 10 to 18 have skin polystyrene and core polypropylene					
20	5.47	5.47	40	41/24	100 (10 s)
22	54.7	5.47	40	38/28	100 (10 s)
Specimens 20 and 22 are skin polypropylene and core polystyrene					
23[a]		5.47	40		100 (10 s)
Only one injection unit was used for making specimen 23. This procedure is considered as the normal injection molding					
26[a]	5.47	5.47	40	39/31	100 (10 s)

[a]Polypropylene was injected for both skin and core for sample No. 26. No. 26 is different from No. 23 in that two injection units were used instead of one.

polystyrene/core polypropylene on the B-cut (FD–ND plane) samples from mold side surface to polypropylene side surface. The birefringence of these samples were measured with a Leitz Laborlux 12 POL S microscope with four-order Berec compensator. Through observation, it was found that the local symmetry axis direction varies with distance from the surface. In order to determine the birefringence, the local direction of the symmetry axis was determined first and birefringence was measured with respect to this local symmetry axis. Therefore, the values reported here represent the maximum birefringence at each location measured.

The value of optical retardation, Γ (mm), was obtained using the calibration chart provided by the manufacturer of the compensator. The birefringence was obtained using the equation below:

$$\Delta n_{13} = \frac{\Gamma}{d}$$

where d is the thickness of the sample (mm).

2.5. Wide angle X-ray diffraction (WAXD) studies

2.5.1. Microbeam-WAXS

Microbeam-WAXS patterns of the B-cut were taken in selected locations from skin to core using the matrixing microbeam X-ray camera (MMBX) developed in our laboratory [30]. The camera was connected to the Rigaku RU–200B rotating anode X-ray generator operated at 40 kV and 150 mA. The CuK_α beam, having a 100 μm diameter, was obtained using a nickel foil monochromator and a pinhole collimator. The WAXS film patterns were digitized using a 12-bit CCD Photometrics camera, Model CH1. Before making quantitative measurement from the digitized images they need to be corrected for non-linearity of X-ray film as well as the response of the CCD camera. These corrections were done with the help of neutral density filters and a series of exposed X-ray films. The non-linearity of the X-ray film to the real intensity of the X-ray is calibrated separately. Details of this calibration procedure are given in Ref. [31]. In order to quantify the orientation of the *a*, *b*, and *c* crystallographic axes, we assumed that within the probing range of the 100 μm X-ray beam, fiber symmetry exists. Then, we determined the orientation of these axes with respect to the local symmetry axis which may not necessarily be along the flow direction particularly in the interior of the parts. In order to do this we used azimuthal intensity profiles of monoclinic α (110) and (040), and hexagonal β (300) planes. For the monoclinic α phase, Wilchinsky's geometrical rule was used to obtain the $\langle\cos^2\chi_{c,z}\rangle$ value from

$$\langle\cos^2\chi_{c,z}\rangle = 1 - 1.099\langle\cos^2\chi_{110,z}\rangle - 0.901\langle\cos^2\chi_{040,z}\rangle$$

as described in Alexander [32]. And using

$$f_{a,z} = \frac{1}{2}\left(3\langle\cos^2\chi_{a,z}\rangle - 1\right)$$

$$f_{b,z} = \frac{1}{2}\left(3\langle\cos^2\chi_{040,z}\rangle - 1\right)$$

$$f_{c,z} = \frac{1}{2}\left(3\langle\cos^2\chi_{c,z}\rangle - 1\right)$$

and

$$f_a + f_b + f_c = 0$$

all three orientation factors were obtained. Though this relationship is strictly for crystal systems with orthogonal axes, it is a good approximation for PP. (The β angle of the unit cell is 99.3°.)

For hexagonal β phase it is sufficient to obtain f_a from the azimuthal intensity distribution of the (300) plane and from

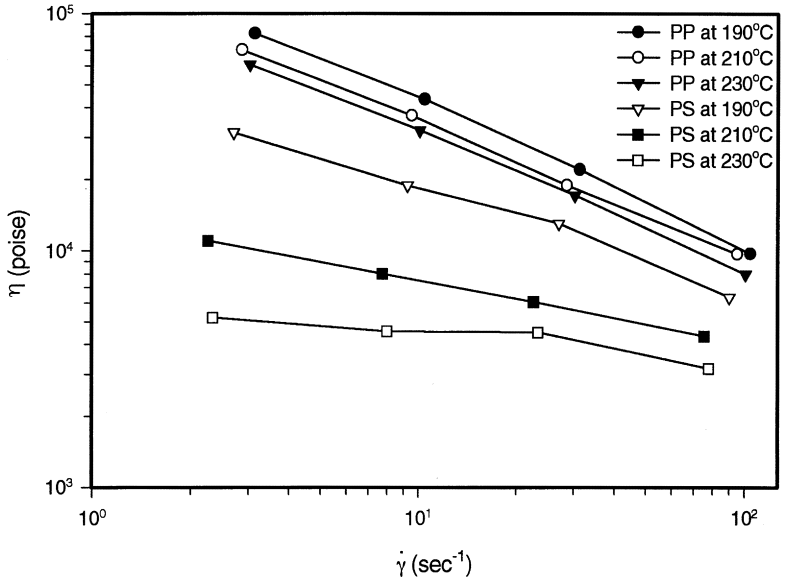

Fig. 3. Viscosity versus shear rate for PS and PP at 190, 210 and 230°C.

the crystal symmetry

$2f_a + f_c = 0$

f_c value is obtained.

2.5.2. Wide angle X-ray pole figures

For pole figure analyses, small rectangular samples with 0.5 mm × 0.5 mm × 2.0 mm dimensions were cut with the long axis along the flow direction for sample No. 16. The samples were mounted on a 0.5 mm diameter polystyrene bristle with the long axis (FD) parallel to the bristle axis. WAXS pole figures for the (110) and (040) planes were obtained using an automated quarter circle GE goniometer with $\Delta\chi = 5°$ and $\Delta\phi = 10°$ (rotation about the spindle axis) using step scanning mode. The GE XRD-6 X-ray generator equipped with a copper target tube provided the X-ray beam that was monochromatized using a detector side graphite crystal.

3. Results and discussion

3.1. Melt viscosity

The viscosity of polystyrene and polypropylene used in this research as a function of shear rate is shown in Fig. 3. At all three temperatures measured, the viscosity of polypropylene is higher than the viscosity of polystyrene. This is particularly true at the chosen processing temperature of 230°C at which all the parts in this research were produced. Although the material typically experiences shear rates in the $10^3\ s^{-1}$ range during processing, the difference in the viscosities of the two polymers at this range would remain substantial as it can be deduced from extrapolation of these two curves to this shear rate range. When the higher viscosity polypropylene is co-injection molded as the outer (skin) layer, the part should exhibit thickness instability at the boundary of the two materials [12]. This in fact was found in this research as discussed below. This relatively high processing temperature was chosen to increase the solidification time of polystyrene thereby minimizing the short shot possibility.

3.2. The geometry of the core material

3.2.1. Polystyrene skin/polypropylene core

The optical photographs of all samples from Nos 10–18, are shown in Fig. 4. The processing conditions of the samples are given on the left and bottom of this figure. The injection speed of the PP phase is indicated on the left column of these boxes (L = low speed, M = medium speed, H = high speed). The mold temperature is indicated on the left column of these boxes. In this figure, the PP core is easily observable through the transparent polystyrene skin. The gate is located at the lower edge of these samples. All the samples molded with low injection speed (Nos 10, 13 and 16) exhibit a blunt flow front, while samples molded with intermediate and high speeds exhibit a ''pointed'' flow front in the polypropylene core resulting in uneven distribution of the polypropylene along the flow direction.

The thicknesses of each phase along the flow direction in the center of the sample was measured and are presented in Fig. 5. High injection speed (No. 12) results in larger accumulation of the polypropylene phase closer to the gate. Conversely, the decrease in the injection speed causes more uniform distribution of the PP core regions along the flow direction, though the effect of the mold temperature on the thickness uniformity is low, but still noticeable, and lower mold temperature results in slightly better distribution of the core along the flow direction.

This behavior is explained schematically in Fig. 6, which shows the skin polystyrene melt front movement in the mold as it is injected first. Two distinct fronts are established during the injection process. The first front is the flow front, which moves with speed V_1. The second is the time front that defines the solid–liquid boundary, which moves towards the interior of the part. This is noted as V_2 and this speed is primarily governed by the local heat flux vector which is primarily controlled by the differences in mold and melt temperatures. The spatial profile of the solid–liquid boundary throughout the part at the end of the filling stage defines the thickness of the frozen-in layer at that time and is the boundary beyond which the nucleation density usually decreases owing to decay of built-up stresses. The regions toward the core remain molten and are further deformed when core polypropylene is injected. This is expected to have a significant influence on the structure developed in the PS skin layer as well as the PP regions near the interface of the two polymers. The complex flow fields during the second injection is illustrated schematically in Fig. 6 for high and low injection speeds. At low injection speed the frozen layer advances further into the core of the sample before the flow front reaches the end of the mold. Since all nine samples discussed in this section have the same volume change of polystyrene/polypropylene, thicker polystyrene at a given location means thinner polypropylene at the same location.

As explained earlier, two fronts are established during the injection molding: the flow front and the solid–liquid boundary. As the solid–liquid boundary moves towards the interior, the effective cross-sectional area, through which the polymer flows, is reduced. This results in increased local fluid velocities for a given constant flow rate defined by the injection unit [33]. As a result, fast injection causes the interior material to accumulate closer to the gate while slower injection forces the core layer to spread in the flow direction since at lower speeds, the frozen layer advances inwardly, decreasing cross-sectional area. As a result, the polypropylene core advances forward in the interior of the samples.

The thickness variation, among different mold temperatures at the same injection speed, is less significant as seen

in Fig. 5. This result also ensures the fact that core polypropylene has the deciding effect on the thickness variation of the skin polystyrene. It can be concluded that injection speed has the most influence on the geometry of the interior samples when both materials are at the same temperature. In order to obtain uniform distribution of the core material, these results indicate that lower injection speed should be used. Similar effects can also be obtained by increasing the viscosity of the polystyrene by reducing its melt temperature. However, this was not done in this research.

3.2.2. Polypropylene skin/polystyrene core

The samples No. 20 and No. 22, which have polypropylene injected first to form the skin regions and polystyrene to form the core, exhibit a completely different core geometry, as shown in Fig. 7, as compared with the skin polystyrene samples shown earlier in Fig. 4. Fig. 7 shows that the distribution of the core polystyrene is uneven across and along the flow directions. In this figure, one half of the skin PP was removed for clear observation of the PS core. This behavior is consistent with the earlier reports where this type of unstable behavior is observed when lower viscosity material is injected into a higher viscosity molten pool [11,12]. Even though no burst through was observed in our study of skin polypropylene/core polystyrene, the thickness variation along and across the flow direction was large.

3.3. Polystyrene birefringence

Birefringence development in straight injection molded atactic polystyrene was first studied by Ballman and coworkers [34,35]. Their studies revealed that polystyrene exhibits dog-eared birefringence profiles across the thickness of the molded parts with the absolute maximum

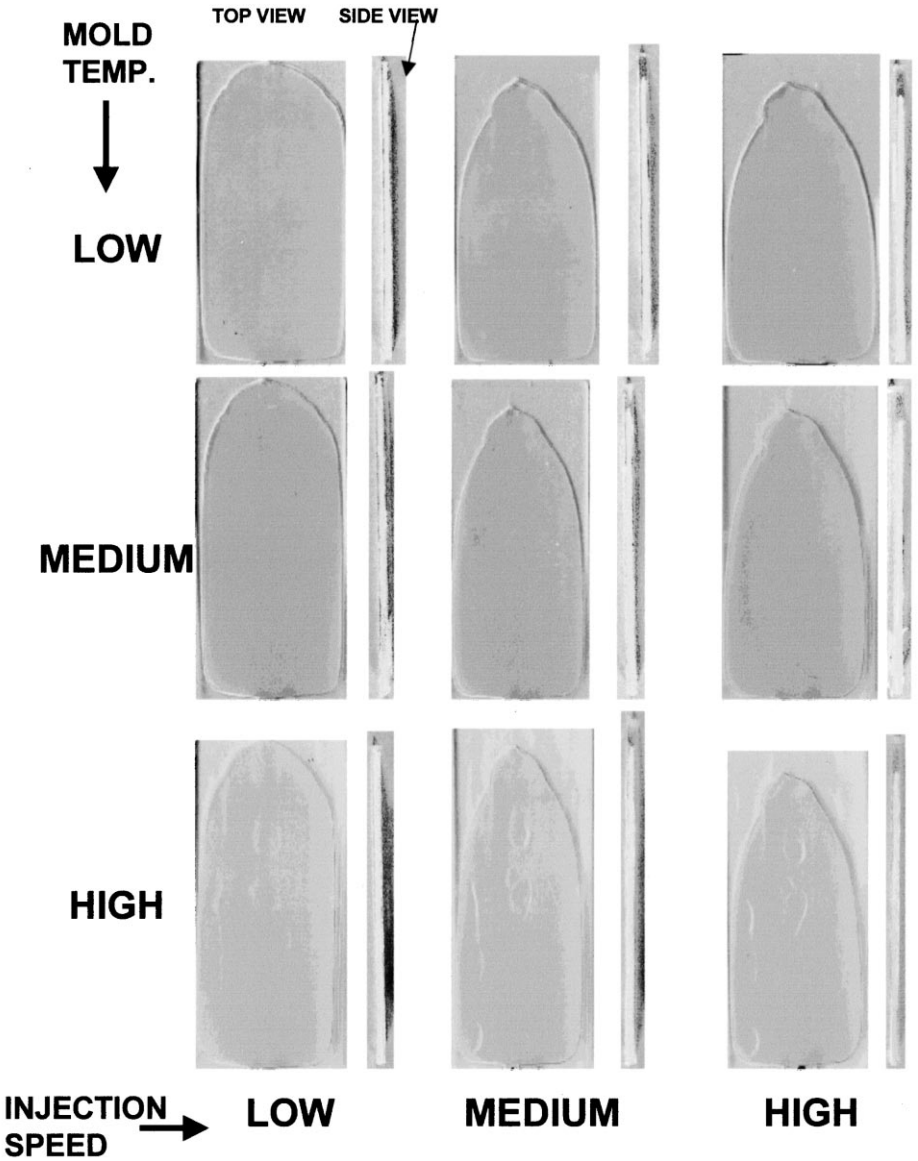

Fig. 4. Interfacial geometry of polystyrene skin/polypropylene core samples (No. 10 and No. 18).

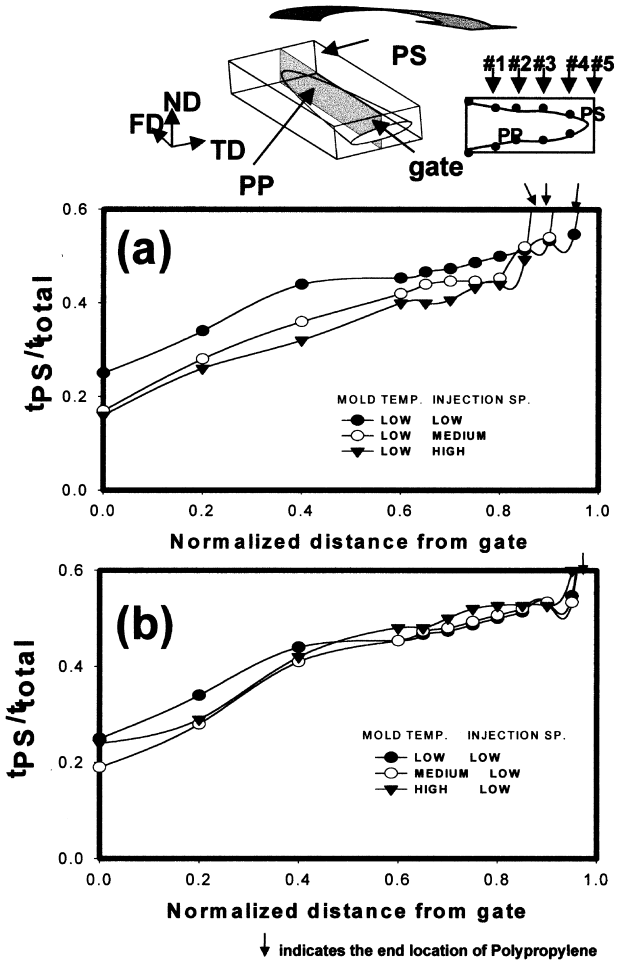

Fig. 5. The normalized thickness distribution of phases under (a) varying injection speed, (b) varying mold temperature.

of the birefringence being at intermediate regions close to the skin. The center of the parts exhibited typically little or no birefringence due to rapid decay of stresses and developed orientation as a result of slow cooling. This has been confirmed by several other researchers [36–38], but some researchers found the additional maximum near the outer surface [37,38]. There are two main sources for birefringence developed in an injection molded amorphous polymer like polystyrene. One is flow induced birefringence as a result of preferential orientation of the chains in certain directions typically along the flow, and the other is thermal birefringence that is caused by the non-equilibrium density change during inhomogeneous rapid cooling through the glass transition temperature [39].

A birefringence minimum has sometimes been observed between the surface and the maximum value and in the core [40,41]. Birefringence is influenced, by melt temperature, injection speed, mold temperature and packing pressure. Generally increasing the melt temperature decreases the maximum birefringence. This result is because of the fact that increasing the melt temperature drastically reduces the relaxation time of the melt. Therefore, it creates favorable conditions for the relaxation of stresses and birefringence after the cavity filling. Decreasing the injection speed increases the value of maximum birefringence. According to Isayev [42] increasing the flow rate leads to truncation of the long-term tail of the relaxation spectrum of the polymer melt, thus decreasing the effective relaxation time. The second reason is that at the high flow rate, thermal convection dominates over thermal conduction to the cold mold, thus creating the favorable conditions for the relaxation process and retarding the growth of the frozen surface layer.

The effect of the mold temperature on the maximum birefringence is considered in the same manner as the effect

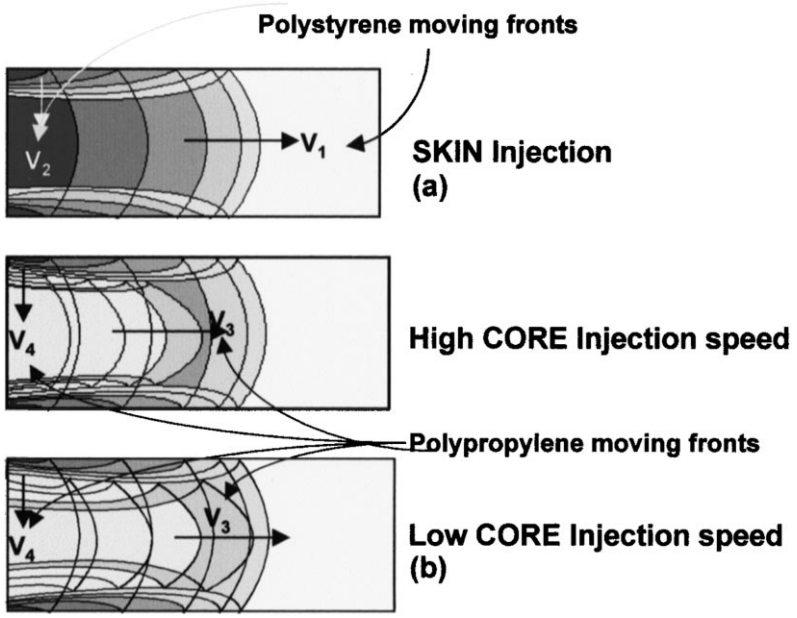

Fig. 6. Flow front movement in the filling stage of (a) skin polystyrene and (b) core polypropylene in the co-injection molding process.

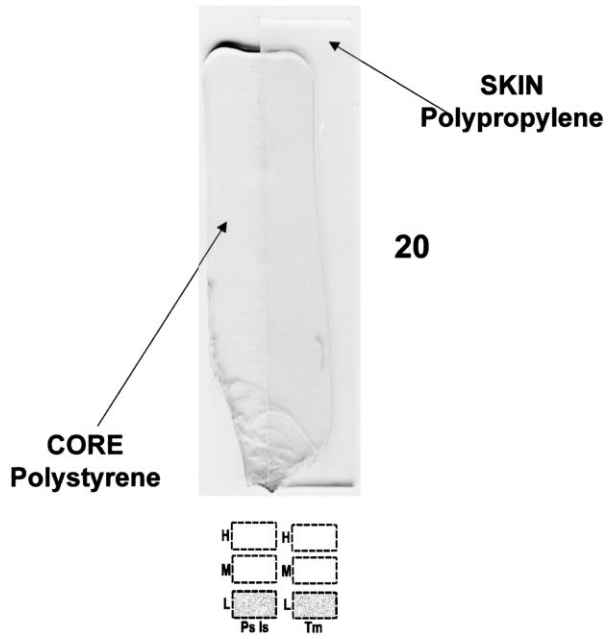

Fig. 7. Optical photomicrograph of sample No. 20 polypropylene skin/polystyrene core. Injection speed of PP = low; mold temperature = low.

of the melt temperature. Increasing the mold temperature decreases the value of maximum birefringence, creating a favorable condition for stress and birefringence relaxation. The packing pressure also plays an important role in creating a second birefringence maximum close to the core. While the birefringence maximum near the wall is formed during the cavity filling, the second birefringence is developed as a result of a rise in normal stress in the packing stage when the core region is still hot. The development of normal stress in layers adjacent to the frozen-in layer in this packing stage should be retarded owing to the long relaxation time.

Due to the extremely low levels of birefringence detected in core polystyrene, as is expected from the high melt temperature, in this study we concentrated only on the birefringence measurements of the skin polystyrene.

3.3.1. Polystyrene skin/polypropylene core

The birefringence of skin polystyrene is summarized in Fig. 8. It should be pointed out that the birefringence values presented here are the maximum birefringence at each location whose local symmetry axis is defined by the extinction angle (tilt angle). In this figure, the birefringence profiles from the mold surface to the PS/PP interface are presented. In each graph the data in each graph represent the results of three injection speeds at constant mold temperature. In all the data, the birefringence first increases, shows a maximum and then decreases towards the inner surface (polypropylene side). However, we do not see a secondary peak near the inner surface, though we do observe an increase in the tilt (extinction angle) near the mold surface and near the PS/PP interface in all samples where the PP core was injected with the slowest injection speed (see the data for sample Nos 10, 13, and 16 for each mold temperature). This is a clear reflection of the evolution of stresses during the injection process. The slow injection allows for the larger penetration of the solidified layers towards the core and the polymer chains ending up in these regions preserve orientation developed during their flow under higher stress conditions better due to

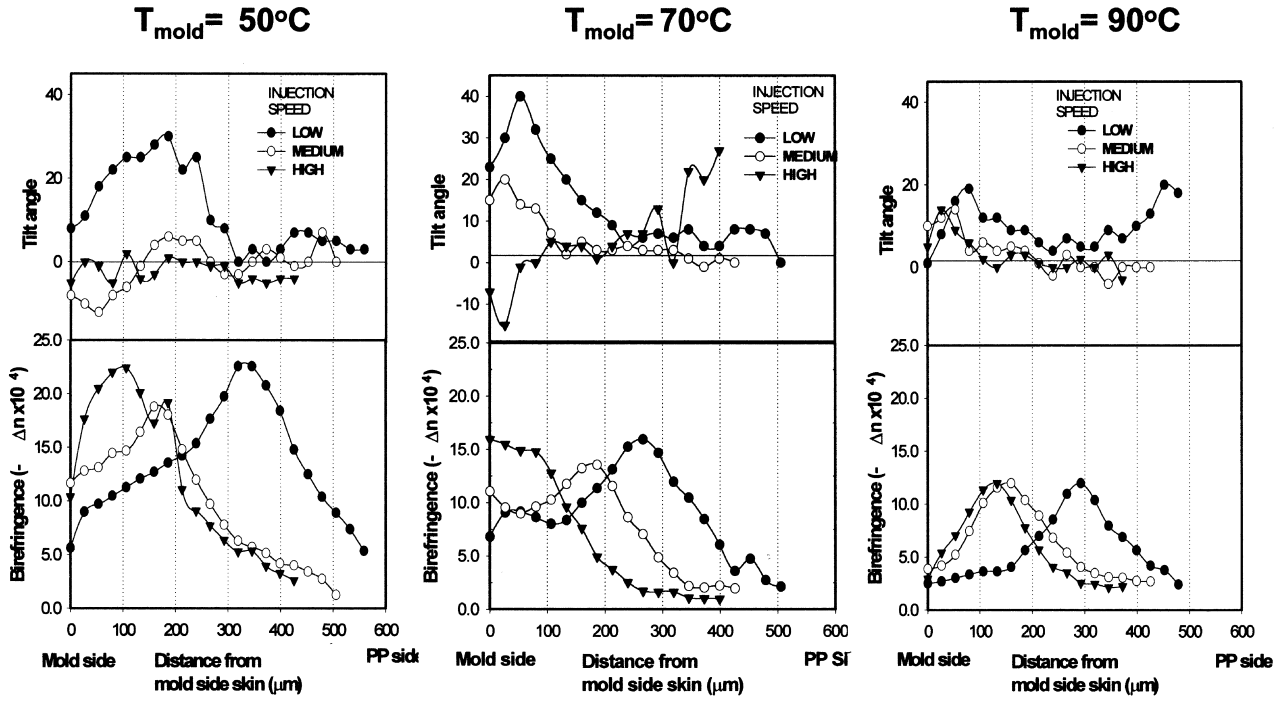

Fig. 8. Birefringence and tilt angle distribution of skin polystyrene molded at three mold temperatures and injection speeds.

the significantly reduced orientation relaxation at lower temperatures [43]. The values of birefringence remaining in all samples are relatively low as a result of the high melt temperature of 230°C used during injection.

The relative location of the maximum birefringence value depends on the core polypropylene injection speed. Increasing injection speed at the same mold temperature shifts the location of maximum birefringence towards the mold wall. Considering the fact that all skin polystyrene has the same injection speed and charge volume, it is reasonable to assume that the birefringence distributions were the same up to the beginning of the PP injection stage. As the injection speed of PP is increased, more of the unfrozen material stays near the gate, locally reducing the PS thickness and thereby moving the birefringence maximum closer to the mold wall. The increase of mold temperature causes an overall decrease of the magnitude of birefringence. It should be noted that the local extinction angles are low at the surface and increase rapidly towards the intermediate regions before reducing to zero at the locations where birefringence maxima are observed.

The effect of mold temperature on birefringence can be observed in Fig. 9. In this graph all samples have the same low injection speed. The increase of the mold temperature significantly reduces the birefringence throughout the thickness and the peak position moves slightly closer to the mold surface. This occurs primarily as a result of a decrease in cooling rates upon increase of mold temperature which decreases the relaxation time.

3.4. Optical microscopy

In injection molding of fast crystallizing materials like PP [44,45], PE [46,47], or POM [48,49], a multi-layered structure is usually observed. This structure is also observed in co-injection molded samples, although there are some differences as described below. First, we will review a typical thermal deformation history that a polymer chain experiences during the course of its travel through the machine components. Typically, a polymer chain experiences high temperature gradients as soon as it enters the sprue section under no slip condition, which occurs as a result of rapid solidification of the skin region. Then a deformation rate gradient is immediately established. The polymer chains that end up at a skin region have usually followed the mid-section of the flowing mass where the shear stresses are at their lowest. They experience the extensional flow at the flow front before being ‘‘slapped’’ against the cold wall. They have very little time to relax to the random coiled state from the acquired orientation levels. These chains experience the highest temperature gradient due to their direct contact with the cold wall.

Owing to the poor thermal conductivity of the polymers, the highest cooling rates are usually confined to the boundaries, and the rate of cooling rapidly decreases towards the interior of the parts. As has been studied in the absence of flow by many researchers [50,51], the crystallizing polymer exhibits a so-called ‘‘transcrystalline layer’’ in which the preferred fast growth direction is primarily along the steepest slope of the temperature gradient.

As the solid–liquid boundary in the filling stage moves inward from the mold, shear crystallized layers of very high nucleation density and lower nucleation density regions are established. The boundary of these two layers is defined from the moment the flow front stops moving at the end of the cavity, thereby suddenly stopping the shearing process throughout the molten path. Once flow stops, the very high shear stresses start decaying. Depending on the local cooling rates, the polymer crystallizes at decaying cooling rates towards the core. This cooling results in the decrease of nucleation density towards the core. In the following section, the layered structure of each molding condition will be described.

3.4.1. Polystyrene skin/polypropylene core

Fig. 10 shows the cross-section of core polypropylene, sample No. 10 (low T_m and low core I_s) and sample No. 18 (high T_m and high core I_s), cut parallel to the flow direction. Polystyrene was removed before these micrographs were taken. Despite the fact that core polypolylene was injected into a still molten polystyrene environment, the skin layer is still observed. Under cross-polarized light the skin region exhibits a uniform extinction angle, indicating there is no spatial variation of local symmetry axes that are

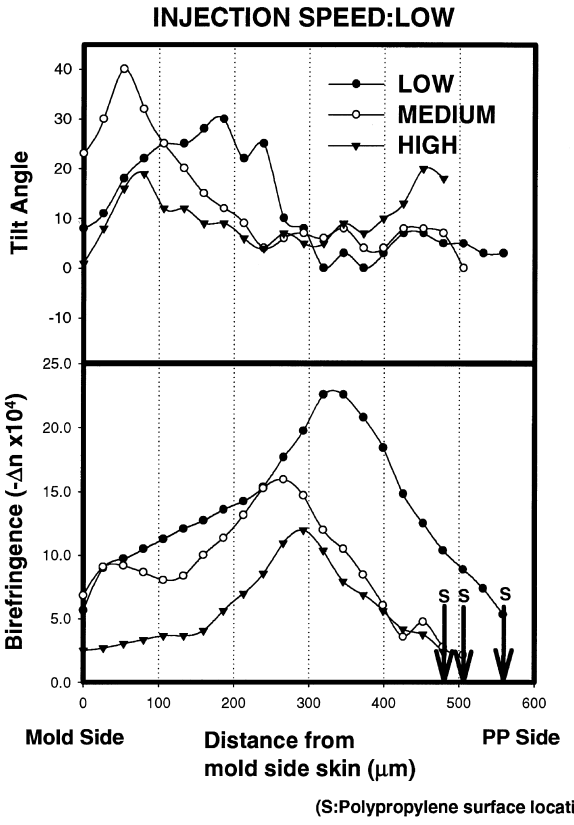

Fig. 9. Effect of mold temperature on birefringence distribution in skin polystyrene (at low injection speed).

pointing in the flow direction. It is also noted that in sample No. 18, which has the highest mold temperature, the skin layer disappears close to the gate.

The next layer towards the core is the shear layer, which consists of highly deformed crystallites. In micrographs with a first-order red wave λ plate (Fig. 11) the crystallites of this layer show a deep blue color, which indicates that crystallites in this layer are highly oriented to the flow direction. The large transcrystalline layer growing perpendicular to the flow direction can be observed as the next layer. This layer has a distinct bright field, which is typical of β crystalline polypropylene. The spherulites of the β crystalline region are known to be type III negative. In location No. 5, the transcrystalline layer becomes the first layer of the core polypropylene. This is more pronounced in the high mold temperature sample. The micrograph of this transcrystalline region reveals that the size of the crystallites in this layer gradually increases toward the center of the sample. The core layer makes up the majority of the rest of the polypropylene. The spherulites in this layer are type Iα spherulites.

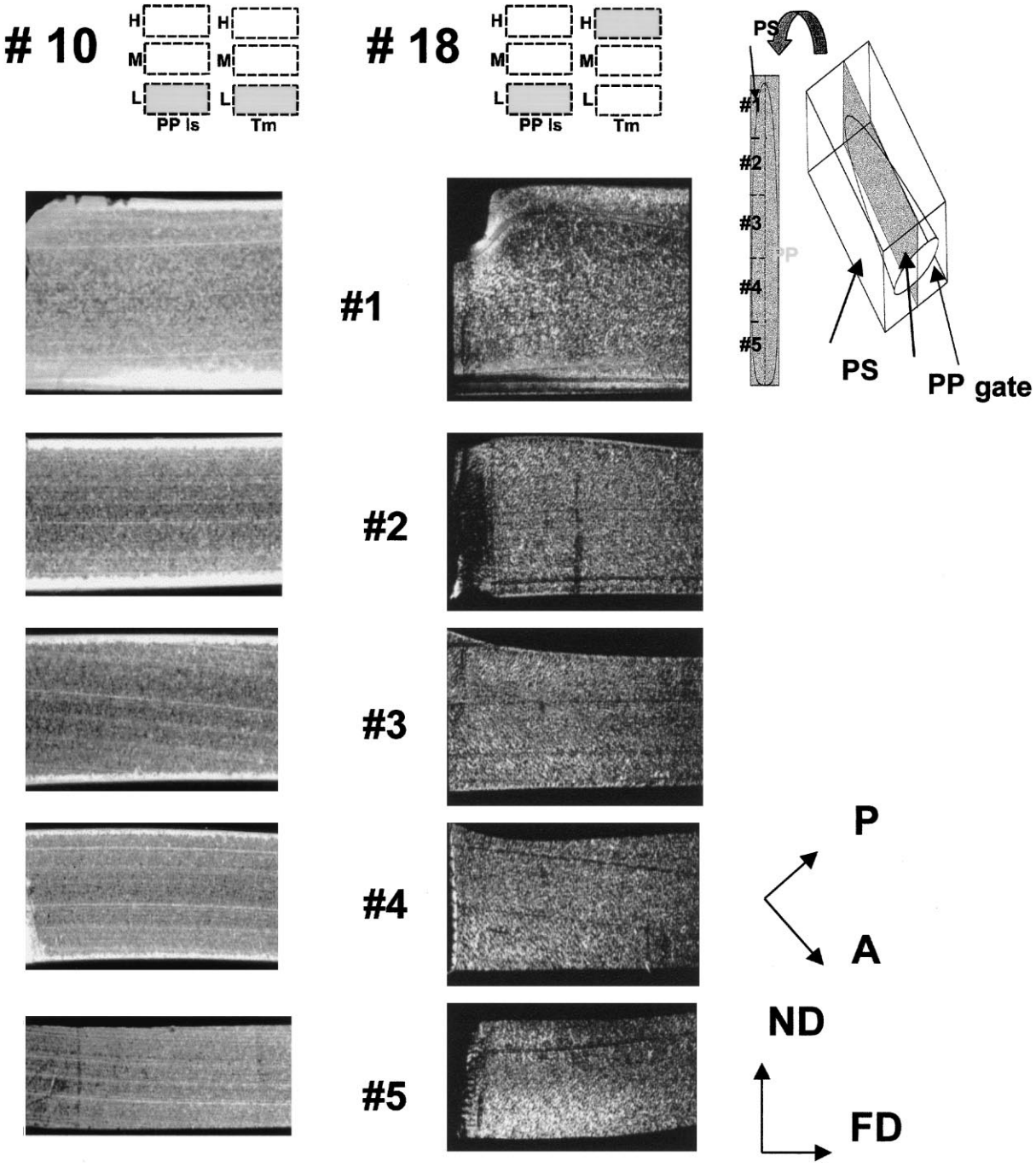

Fig. 10. Optical photomicrographs of the PP core in samples No. 10 and No. 18 cut parallel to the flow direction (FD–ND) plane.

3.4.2. Polypropylene skin/polystyrene core

The samples molded with PP as the skin layer exhibit different layer structures as shown in Fig. 12. Due to the significant shear against the mold wall, the outside polypropylene has little or no core region compared to the center of the polypropylene injected as the core layer. In the latter large, fairly isotropic spherulites are observed.

In Fig. 12, the skin layer is observed just as in straight injection molded samples. The thickness of this layer does not exceed 10 μm. A very large, highly oriented shear layer taking up more than 80% of the total thickness of the sample is observed. The neat transcrystalline layer grows perpendicular to the flow direction along the steepest temperature gradient. The orientation behavior in these regions will be discussed in the following X-ray sections.

3.5. Local orientation behavior studied by microbeam-WAXS

Before discussing the details of X-ray patterns for each condition, typical microbeam-WAXS patterns are presented in Fig. 13 to help in their interpretation. In this microbeam-WAXS experiment of co-injection molding samples, two different polypropylene crystalline modifications were observed, monoclinic α and hexagonal β. The plane indices for β modification are based on the B-cell model [52] of the Turner-Jones et al. classification. While monoclinic α modification is observed in most crystallizations from the melt, hexagonal β can be observed in rapid crystallization from the melt into the temperature range of 120–130°C. Lovinger et al. [50] also showed that the β phase is easily initiated by growth transformation along the oriented α front. At higher orientation levels especially in the shear region, bimodal orientation of the α modification can be seen. In X-ray patterns, (*hk*0) planes of the *c*-axis oriented component appear on the equator and (*hk*0) planes of the a^*-axis oriented component appear on the meridian when the flow direction is vertical. When monoclinic α modification appears with hexagonal β modification, some diffraction peaks are overlapped making it difficult to identify the origin of the peak. For example, the monoclinic α modification (110) plane has a 2θ value of only 0.06° smaller than the hexagonal β modification (210) plane as shown in Fig. 13. As a result, those peaks appear together. As will be shown below, it is possible to distinguish α (040) and β (300) planes on the equator as the *d*-spacing of (300) (5.508 Å) is slightly larger than that of the *d*-spacing of (040) (5.235 Å). It is well known that polypropylene under extensional or shear flow, results in samples exhibiting bimodal orientation [53]. This can be seen in the diagram of monoclinic α modification (left) in Fig. 13. (110) and (130) planes have two distinct peaks, one on the equator, which shows the *c*-axis component contribution and the other one from the a^*-axis component on the meridian. Fig. 13 illustrates why (040) has only one peak on the equator. The unit cell above shows the a^*-axis oriented parallel to the FD and the one below shows the *c*-axis parallel to the FD. It is noticed that the (040) pole points out in almost the same direction in both cases. This observation is the reason why only one peak is observed for (040) planes.

3.5.1. Polystyrene skin/polypropylene core at low mold temperature

Although we explored the structural variation by using three different injection speeds at three different mold temperatures, we will present only selected results in the following sections.

The results of the sample molded at low mold temperature with low injection speed are shown in Fig. 14. For all these samples a constant PS injection speed is used.

The sample was cut along the flow direction and microbeam-WAXS patterns were taken at the No. 3 location whose polarized micrograph is also shown in this figure. The left side of the photograph marked as skin is the PS/PP interface. PS layers in the photomicrograph are not shown for clarity. Although the PP is injected into the core of the polystyrene, which provided thermal insulation during the process, it still exhibits orientation gradients particularly near the PS/PP interface as indicated in the WAXS pattern. The first 200 μm from the interface show

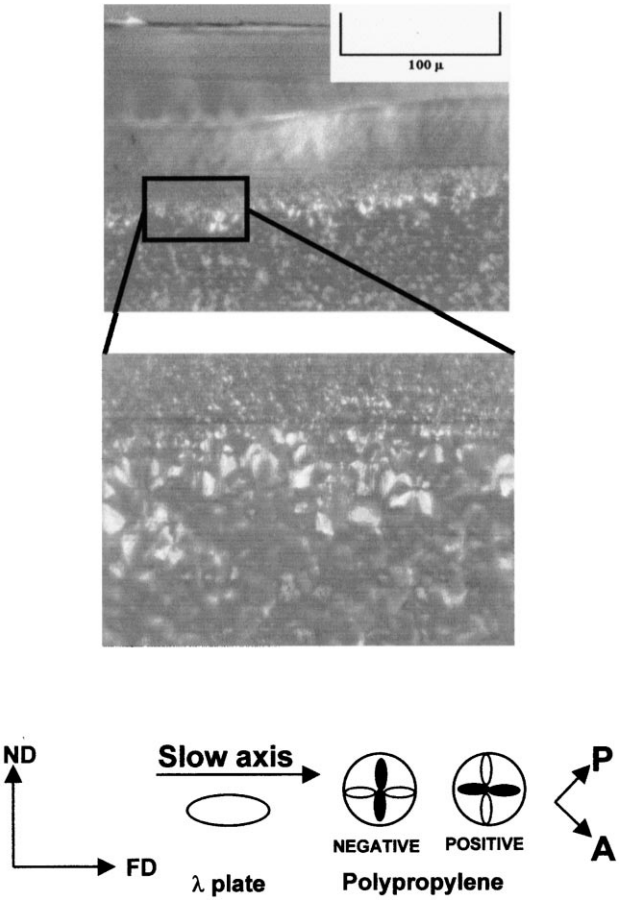

Fig. 11. Optical photomicrograph of injection molded polypropylene near the transcrystalline layer.

highly oriented WAXS patterns. At the surface (position a) the population of the (110) planes is almost exclusively at the meridian indicating that an a^* oriented population dominates. At this position (040) planes are still concentrated on the equator (normal to the flow direction) resulting in a negative value in f_b as indicated in the orientation factor graph shown in the inset. At about 100 μm (position b) from the surface the WAXS pattern shows significant levels of β phase formation as evidenced by the high intensity of (300) planes. This is in accord with the optical picture where a bright band of β crystals is observed between the positions of a and b (indicated by the dashed line in the orientation graph). The increase of injection speed does not change the overall morphological gradients described above, but merely shifts their positions and changes their size. For instance at a middle injection speed shown in Fig. 14(b),

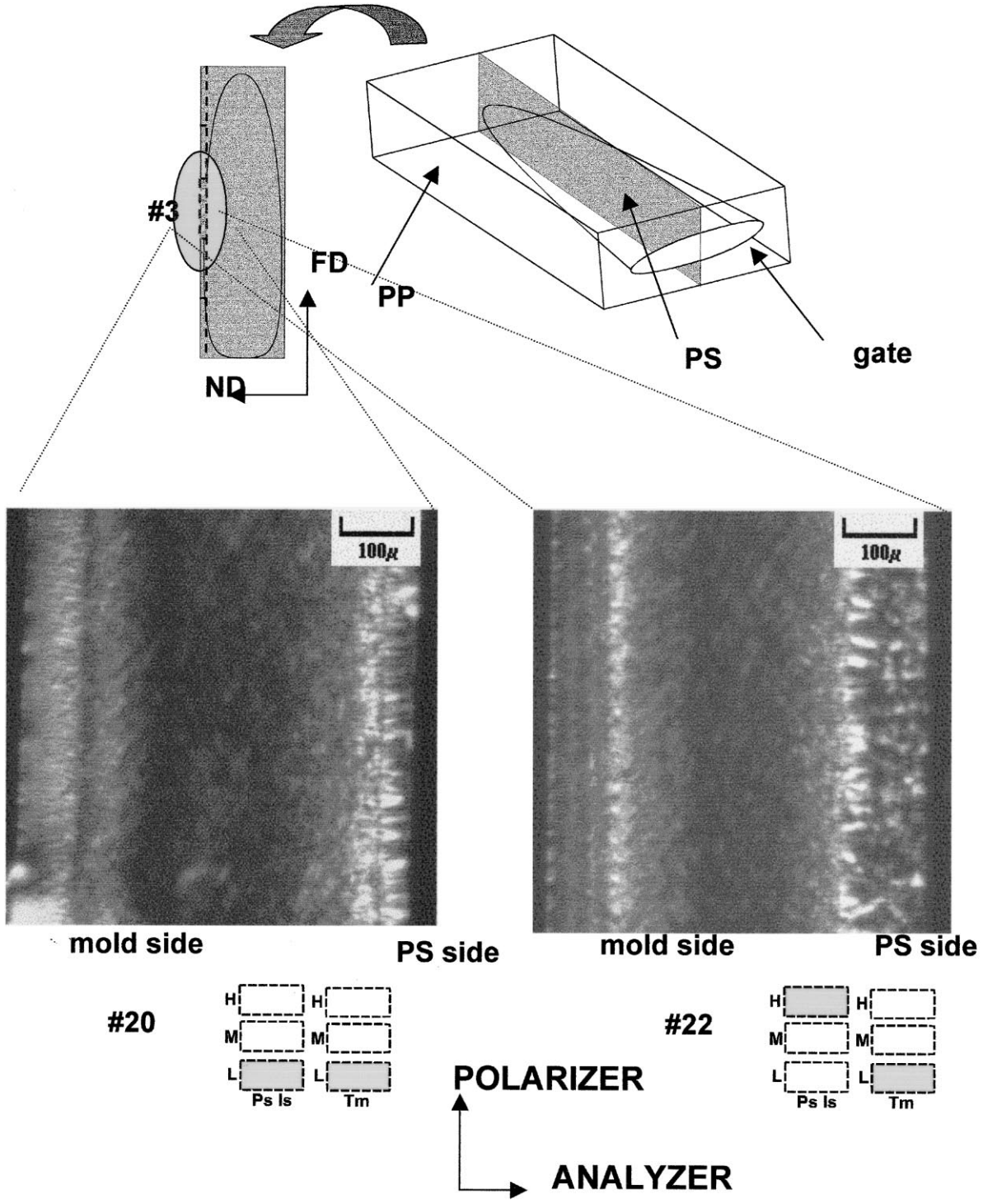

Fig. 12. Optical photomicrographs of the PP skin of samples No. 20 and No. 22 cut parallel to the flow direction (FD–ND) plane.

the transcrystalline growths that contain both α and β phases moves closer to the PS/PP interface and its size increases. This is most possibly as a result of crystallization of the PP at a temperature range of 120–130°C where β phases preferentially nucleate and grow. As we have seen earlier the increase in injection speed causes an even distribution of material along the flow direction which in turn increases the thickness of skin layers at positions near the gate and decreases them at the end of the gate. This increased distance to the surface can certainly cause these regions to cool more slowly resulting in β phase growth. An increase of injection speed further effectively eliminates this layer as evidenced in the optical photomicrograph as well as in WAXS patterns where the (300) peak of the β crystal is no longer observed near the PS/PP interface as shown in Fig. 14(c).

3.5.2. Polystyrene skin/Polypropylene core at the middle mold temperature

As shown in Fig. 15(a)–(c), the overall morphology is similar to that observed at the lower mold temperature with minor variations. At the skin we now observe $c + a^*$ orientation as evidenced by the presence of equatorial (normal to flow direction) as well as meridional peaks. At this mold temperature the β form is observed closer to the PS/PP interface. This is expected as a result of the reduced cooling rate experienced by the polymer. Especially at low and middle injection speeds, hexagonal β peaks are observed in the transcrystalline layer. X-ray patterns indicate that the skin region of sample No. 14 [Fig. 15(b)] has only the hexagonal β phase which disappears towards the core and gives way to the α form. Interestingly the transcrystalline layer that is near the interface disappears at the highest injection speed and randomly dispersed β spherulites are observed throughout the cross-section. However, a closer inspection of the polarized light micrograph reveals that there is an increased proportion of β form spherulites throughout the thickness of the sample. This is possibly an ndication of increased melt temperature due to shear heating at elevated injection speeds.

3.5.3. Polypropylene skin/polystyrene core

When polypropylene is injected first to form the skin layer the level of orientation observed becomes quite substantial as can be observed in Figs 16 and 17. The polarized light micrographs are taken with polarizer and analyzer directions parallel

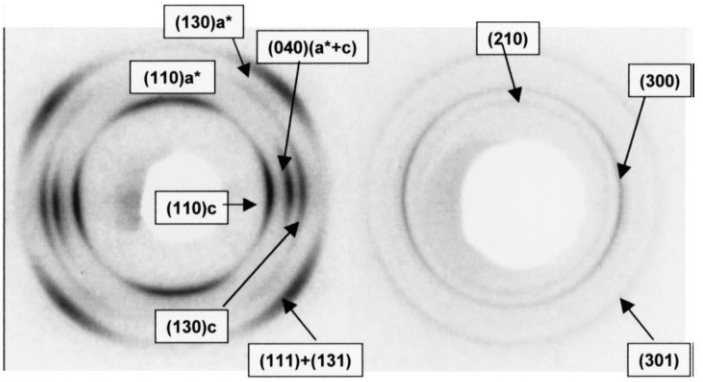

α modification

Intensity	(hkl)	d(A)	2θ
S-MS	110	6.274	14.11
MS	040	5.235	16.93
M	130	4.786	18.53
M	111	4.162	21.34
VW	131	3.628	24.52

β modification

Intensity	(hkl)	d(A)	2θ
M	210	6.245	14.17
VVS	300	5.508	16.08
VS	301	4.200	21.14

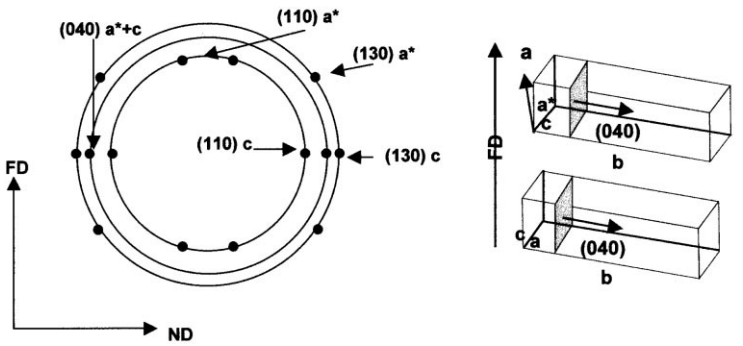

Fig. 13. Typical WAXS patterns of α *abd* β modifications of polypropylene.

to the edges of the photographs and they show the sample from the mold surface to the PS interface and PS layers not shown.

At low injection speed the local symmetry axis shows a significant tilt as indicated qualitatively on the WAXS patterns of the surface layer (position a) and quantitatively as the tilt angle that is equal to 40° tilted towards the core from the (0° = flow direction) in the graph at the inset. This pattern also shows that orientation levels with respect to this local symmetry axis are quite high and no a^* orientation is observed at the meridian. The same is also true at 100 μm from the mold surface (position b). These regions appear brighter in the optical micrograph as the local symmetry axis is tilted away from the polarizer and analyzers. At location c, which is 200 μm away from the mold surface,

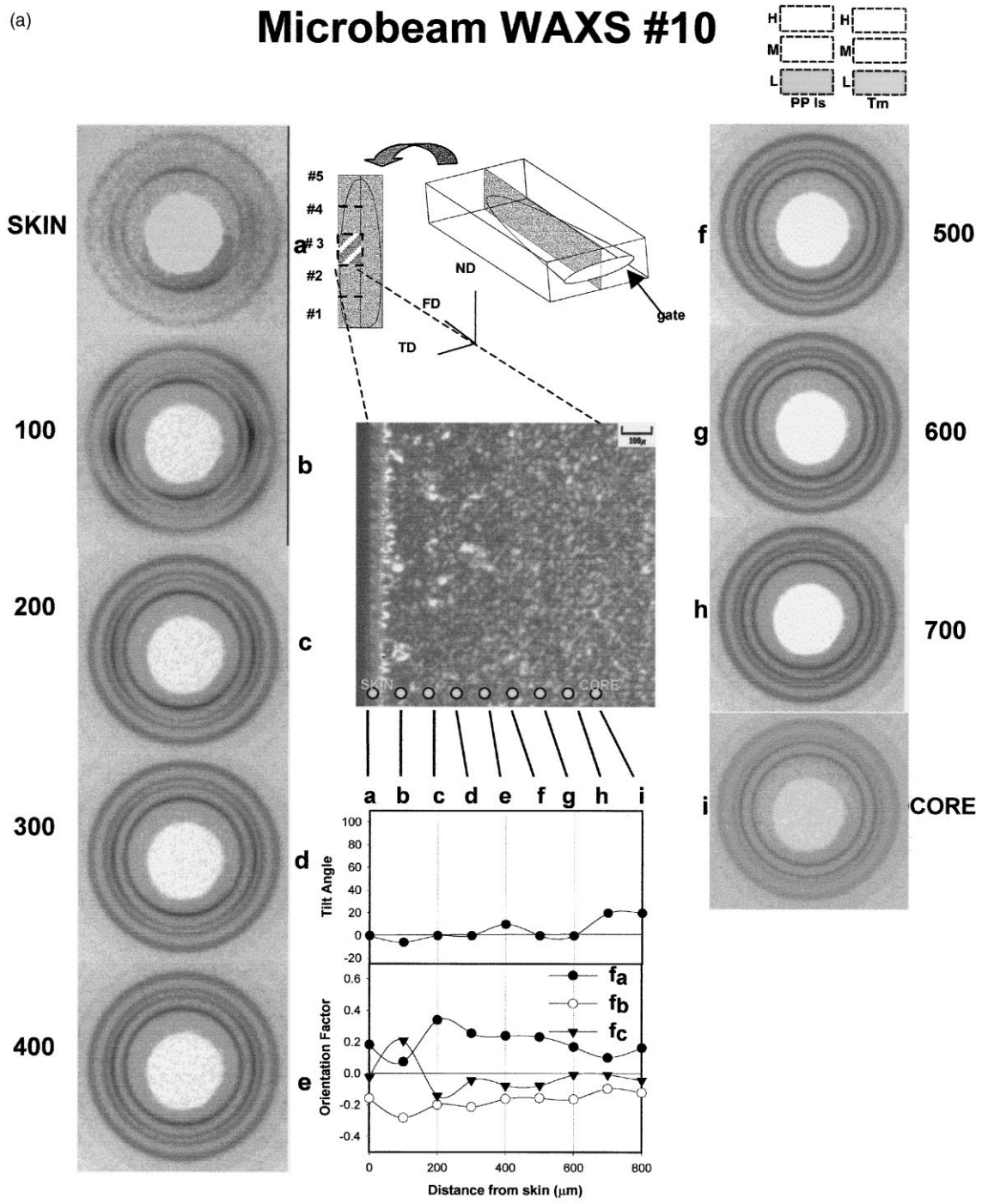

Fig. 14. (a) Microbeam-WAXS patterns, optical photomicrographs and orientation factors for the PP core sample molded at low mold temperature with low injection speed. (b) Microbeam-WAXS patterns, optical photomicrographs and orientation factors for the PP core sample molded at low mold temperature with medium injection speed. (c) Microbeam-WAXS patterns, optical photomicrographs and orientation factors for the PP core sample molded at low mold temperature with high injection speed.

the regions also appear brighter in the photomicrograph but this position shows tilting towards the mold surface. This is a clear result of the complex flow history imposed by the fountain flow as shown by a number of researchers including Mavridis et al. [54]. The interior of the micrograph appears dark as the symmetry axes are all parallel to the vertical edge of the sample (along the flow direction) as also seen in the WAXS patterns. The β phase that was absent in the first 250 μm begins to appear at position d and increases in proportion and at the inner interface it completely dominates the local structure. At positions h and l the local structure is a highly directionally grown transcrystalline region. The WAXS pattern at position l (800 μm) shows distinct (300) β peaks on the equator and (210) β peak on the meridian. The orientation factors determined from these patterns indicate that the highest *c*-axis orientation is observed at about 200 μm from the surface and *a*-axis orientation is negative at the mold surface and becomes slightly positive at

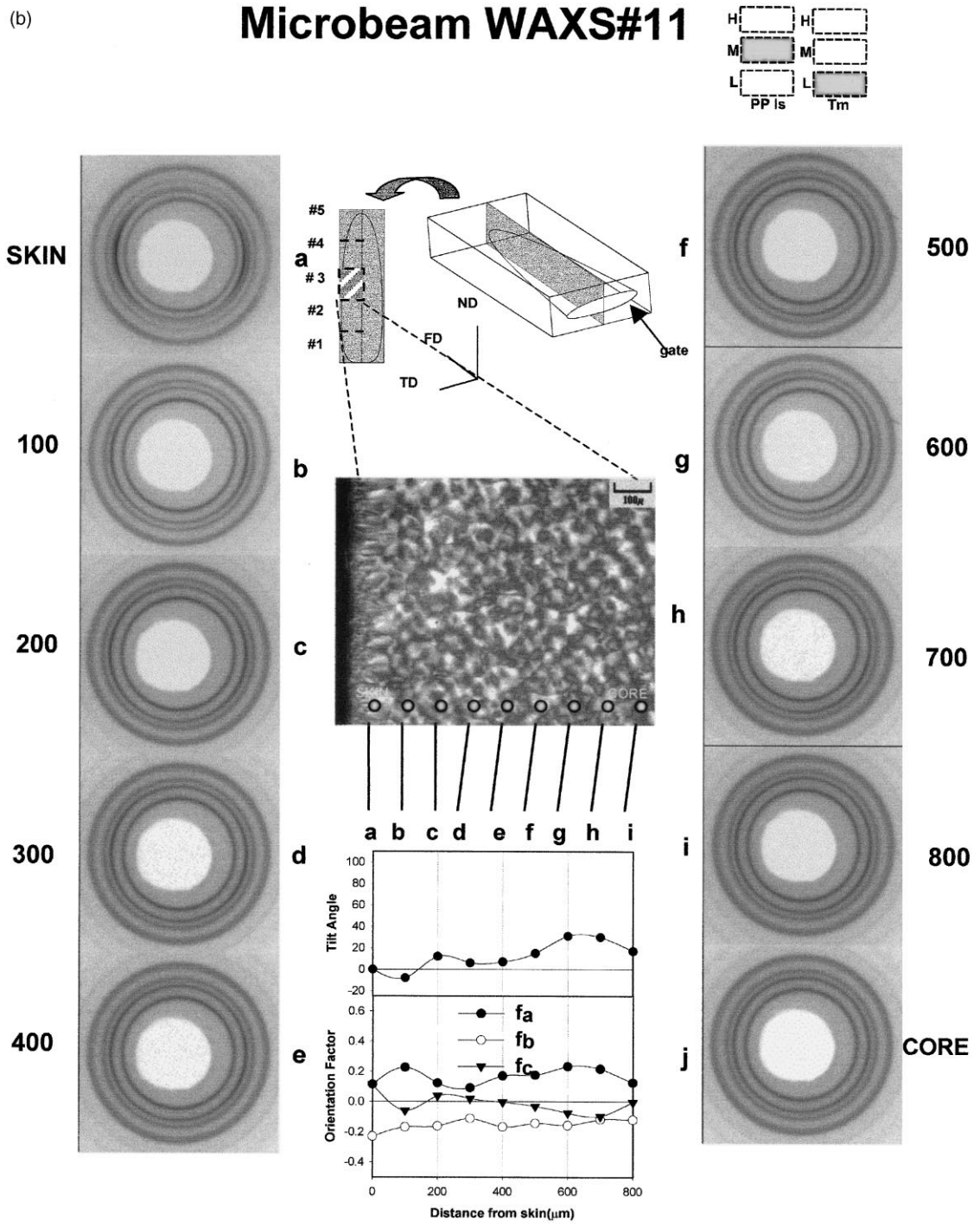

Fig. 14 (*continued*)

the PP/PS interface while *b*-axis orientation remains negative throughout the thickness.

The increase of injection speed has a number of effects on the local structure. The β phase is observed throughout the thickness of the sample although its proportion continuously increases towards the PS side. The orientation character $c + a^*$ orientation is observed throughout the sample and position g is almost exclusively β phase as also revealed in the optical observation. Although the mold surface has higher orientation levels in this sample this rapidly decays towards the PS side possibly as a result of a higher temperature build-up at elevated shear rates.

In order to quantify the *c*-axis orientation versus the a^*, the corresponding equatorial and meridional peaks in the azimuthal direction were separated using a peak separation program and the ratios of their areas are plotted in Fig. 18(a). The a^*-axis oriented polypropylene gradually increases

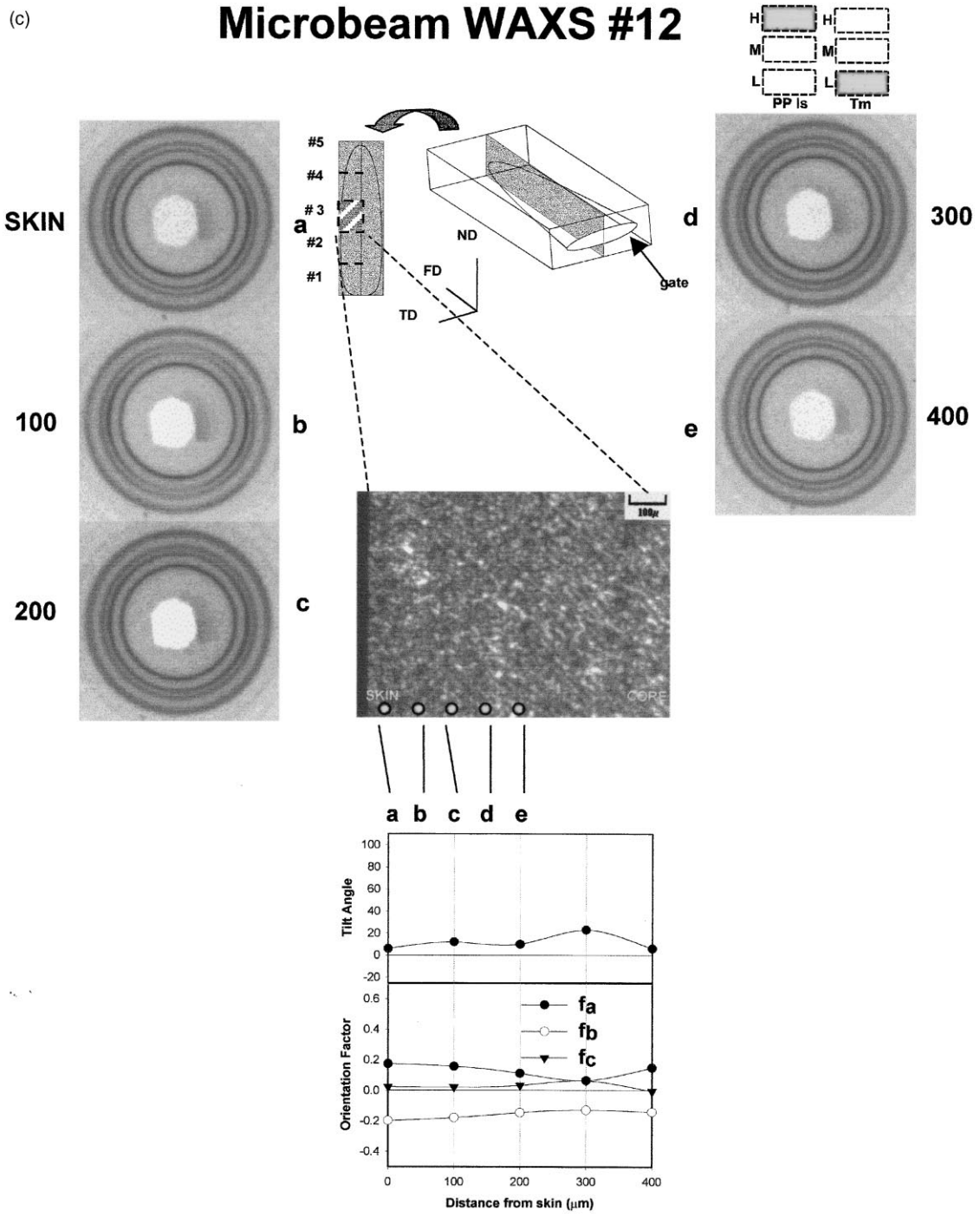

Fig. 14 (*continued*)

from the mold side surface to the polystyrene side surface reaching a maximum value near the transcrystalline layer in which about 75% are the a^*-axis component. As discussed earlier in this section, the hexagonal β component has a diffraction peak of (210), which appears on the meridian. This peak coincides with the meridional peak of monoclinic α modification (110), which may result in an overestimation of the a^*-axis oriented proportion as the fraction of the β phase increases. The X-ray pattern shows only the hexagonal β crystalline due to the absence of (040) and due to presence of (210) on the meridian.

We also plotted the chain axis orientation factor of the β phase in Fig. 18(b). Skin polypropylene showed the hexagonal β phase in most of the locations. In normal injection molding this β phase appears sporadically in the boundary between shear and core layer. Therefore, a quantitative orientation measurement along the thickness direction was rather difficult. Owing to the nature of the growth habit in the transcrystalline layer, this phase has its growth direction along the steepest temperature slope. As a result, a fairly high level of *c*-axis orientation in both samples was observed. The *c*-axis orientation factor has its maximum

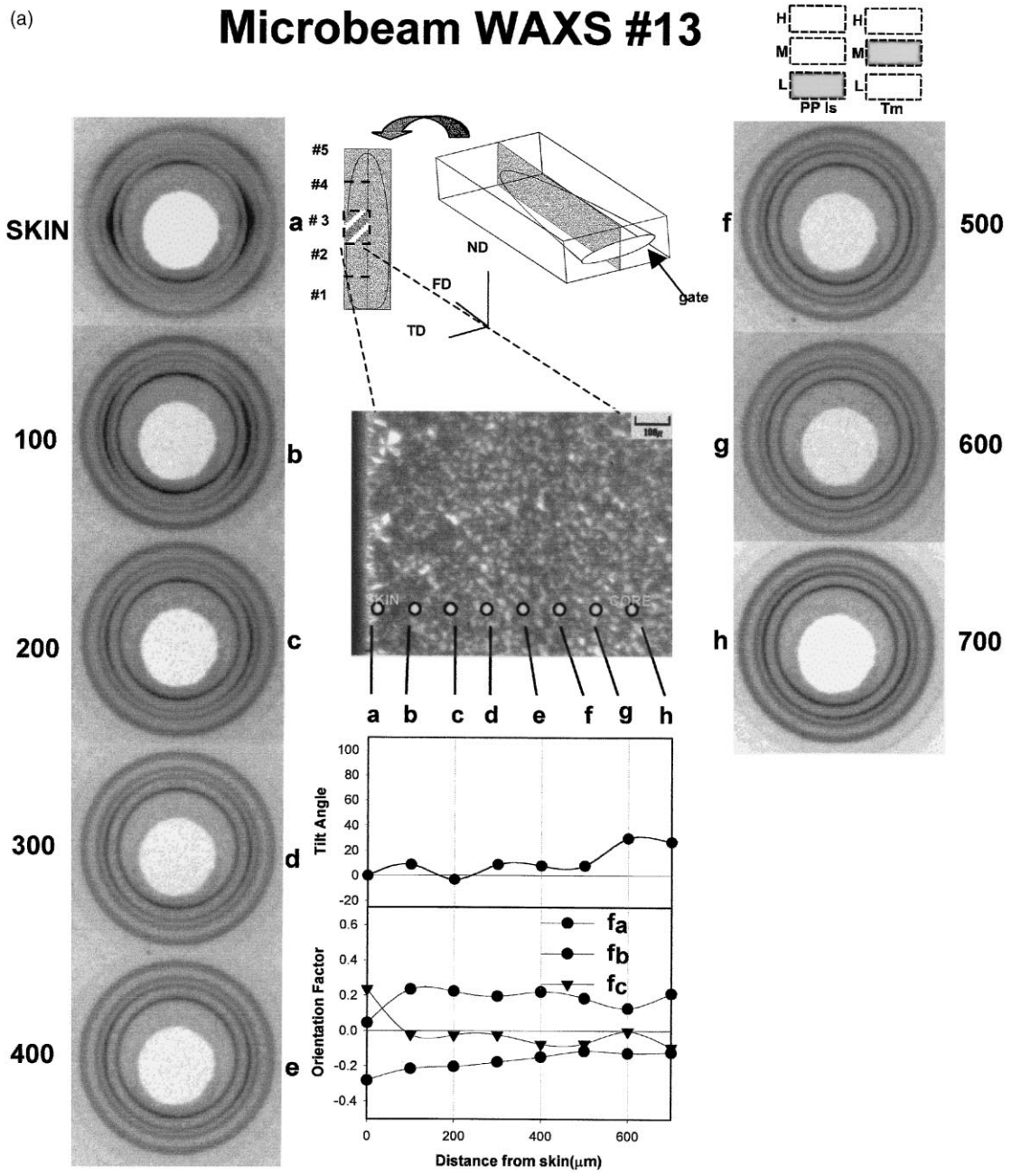

Fig. 15. (a) Microbeam-WAXS patterns, optical photomicrographs and orientation factors for the PP core sample molded at medium mold temperature with low injection speed. (b) Microbeam-WAXS patterns, optical photomicrographs and orientation factors for the PP core sample molded at medium mold temperature with low injection speed.

value in the transcrystalline layer and in the case of sample No. 22, there is another maximum in the mold side skin surface where another population of transcrystalline layers is clearly observed in the micrograph.

3.5.4. WAXS pole figures

As explained earlier, WAXS pole figures of (110) and (040) reflections were taken in the skin and the core of sample No. 16 at location No. 1. The optical photomicrographs of the b-cuts of the regions from No. 1 to No. 4 in increasing distance from the gate are shown in Fig. 19. These b-cuts are shown from the center symmetry plane (right-most position on the pictures) to the left end of the sample. In addition to the wealth of information that can be observed in these micrographs we noticed that the left ends of these cuts exhibit brightly oriented regions that are tilted towards the core. These regions appear optically brighter as a result of their tilt away from the polarizer and analyzer axes. We took two samples, one near the skin and one near the core, to investigate this tilting behavior. The result is shown in Fig. 20.

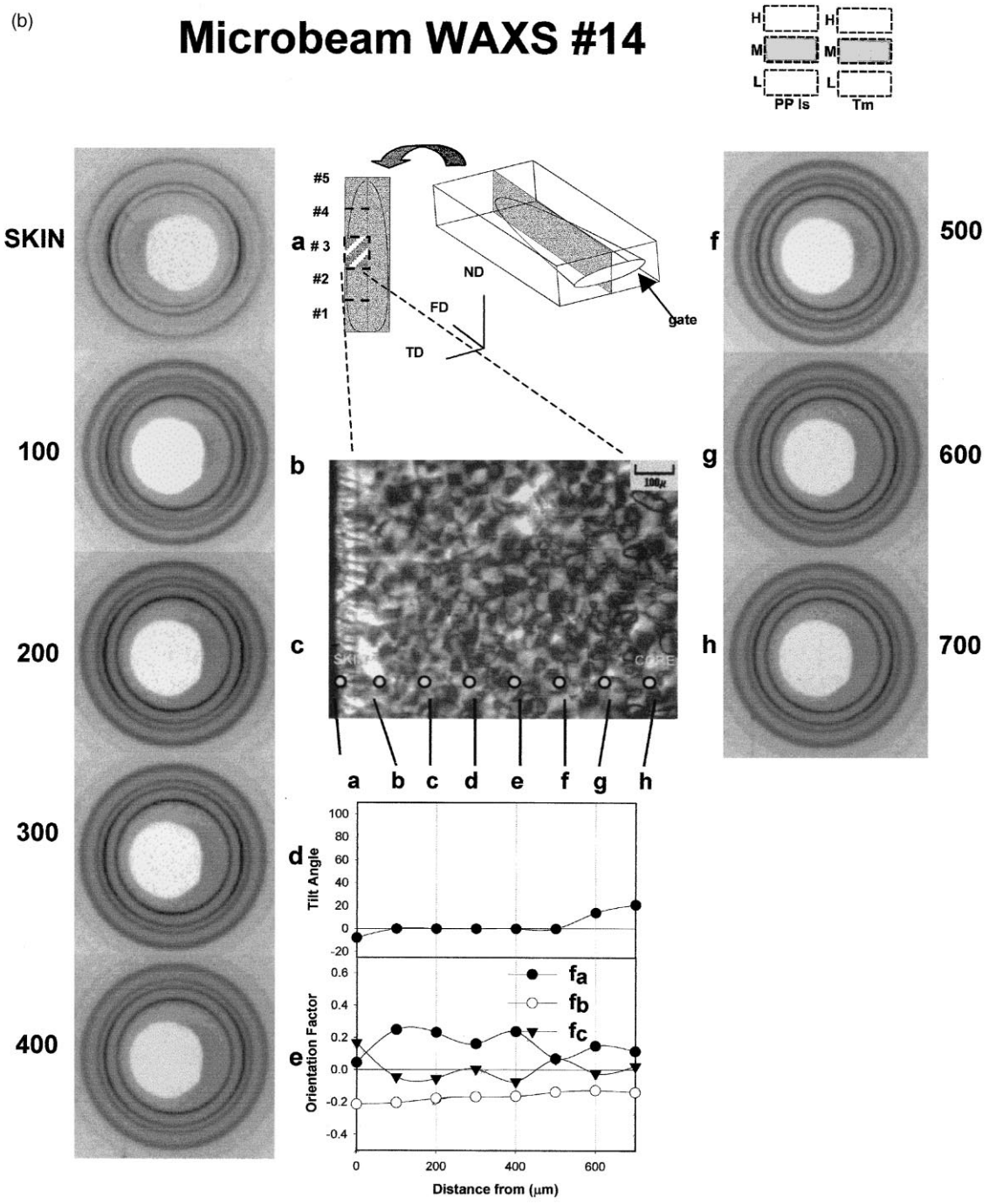

Fig. 15 (*continued*)

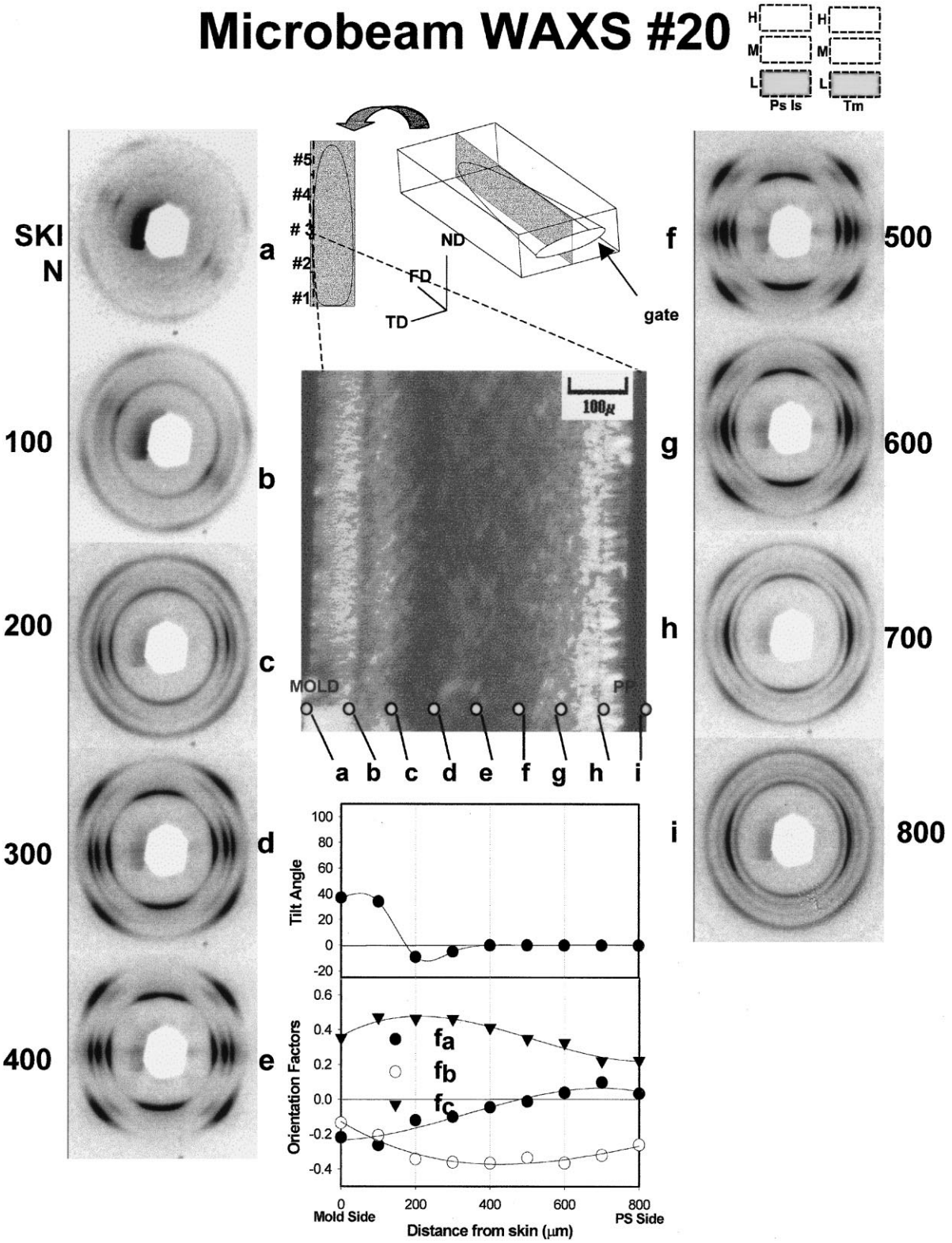

Fig. 16. Microbeam-WAXS patterns, optical photomicrographs and orientation factors for the PP skin molded at low mold temperature with low injection speed.

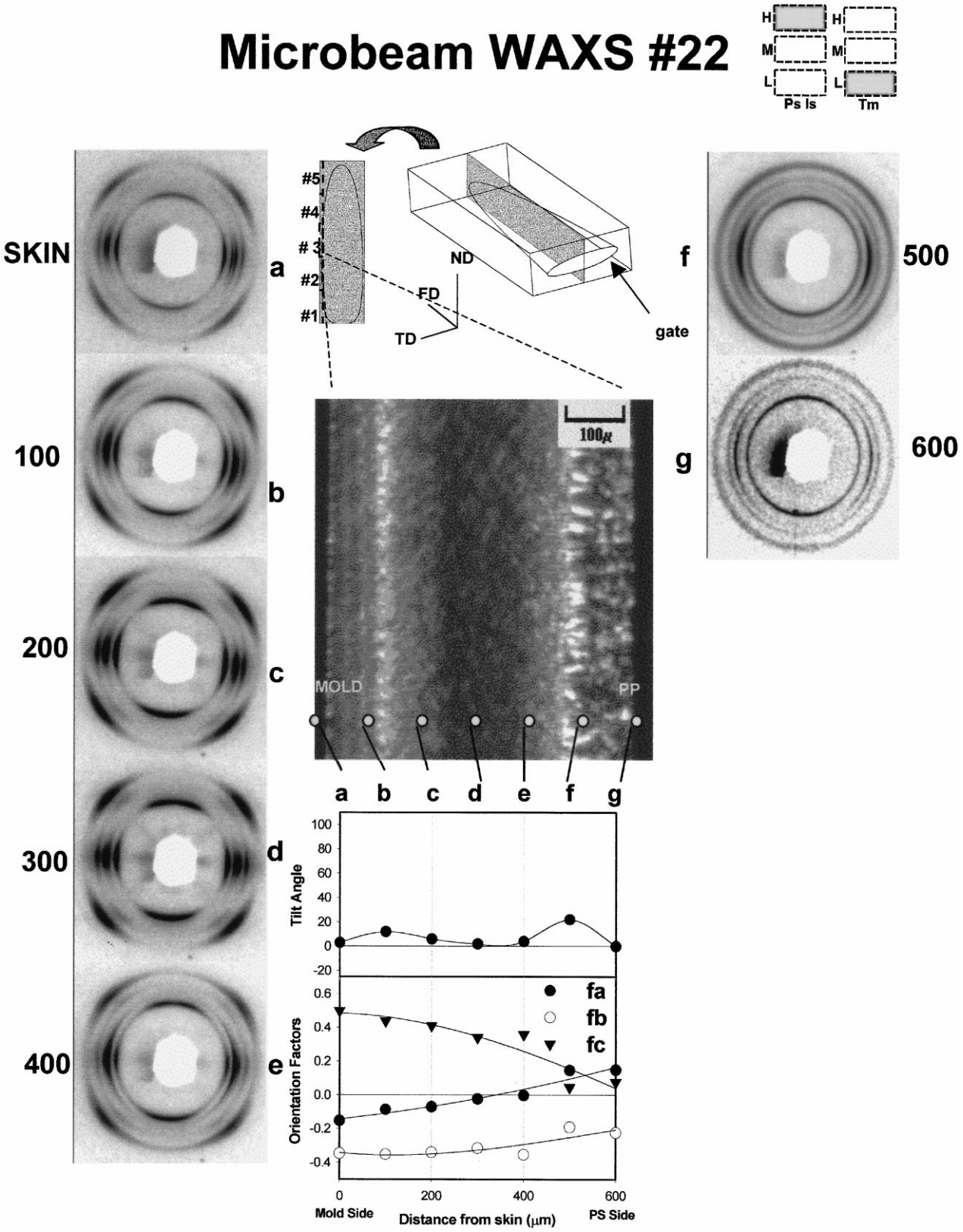

Fig. 17. Microbeam-WAXS patterns, optical photomicrographs and orientation factors for the PP skin sample molded at low mold temperature with high injection speed.

In Fig. 20(a), on the left, is a pole figure obtained for the (110) reflection of polypropylene recorded at $2\theta = 14.1°$. In this figure, the central region of high intensity lies parallel to the direction of the flow, representing the a^*-axis oriented component. In the same figure, the arc-shaped cap on the bottom left part of the pattern shows the contribution of the *c*-axis orientation.

It is usually the case that if there is no tilt angle involved, the preferred direction of the axis of rotational symmetry of the *c*-axis oriented component is exactly parallel to the flow direction. Then two of the arc-shaped caps should be observed 180° apart. The fact that significant tilt was involved in the *c*-axis oriented component and the high level of the a^*-axis orientation (low level of *c*-axis oriented species), makes it hard to find the other cap on the other side of the corner. Although the intensity is low, a non-zero value of relatively high intensity was found in that region.

The (040) reflection of polypropylene recorded at $2\theta = 17.1°$ is shown to the right. Both a^* and *c*-axis oriented components contribute to give the pattern. The (040) pole does not show transverse isotropy—instead it is preferentially oriented close to the transverse direction, but with an approximately 20° tilt angle. The core region pole figure of (110) planes (left) shows a preferential orientation of the a^* while the *c*-axis component is not observed. The pole figure of (040) (right) shows a very broad pole distribution in the

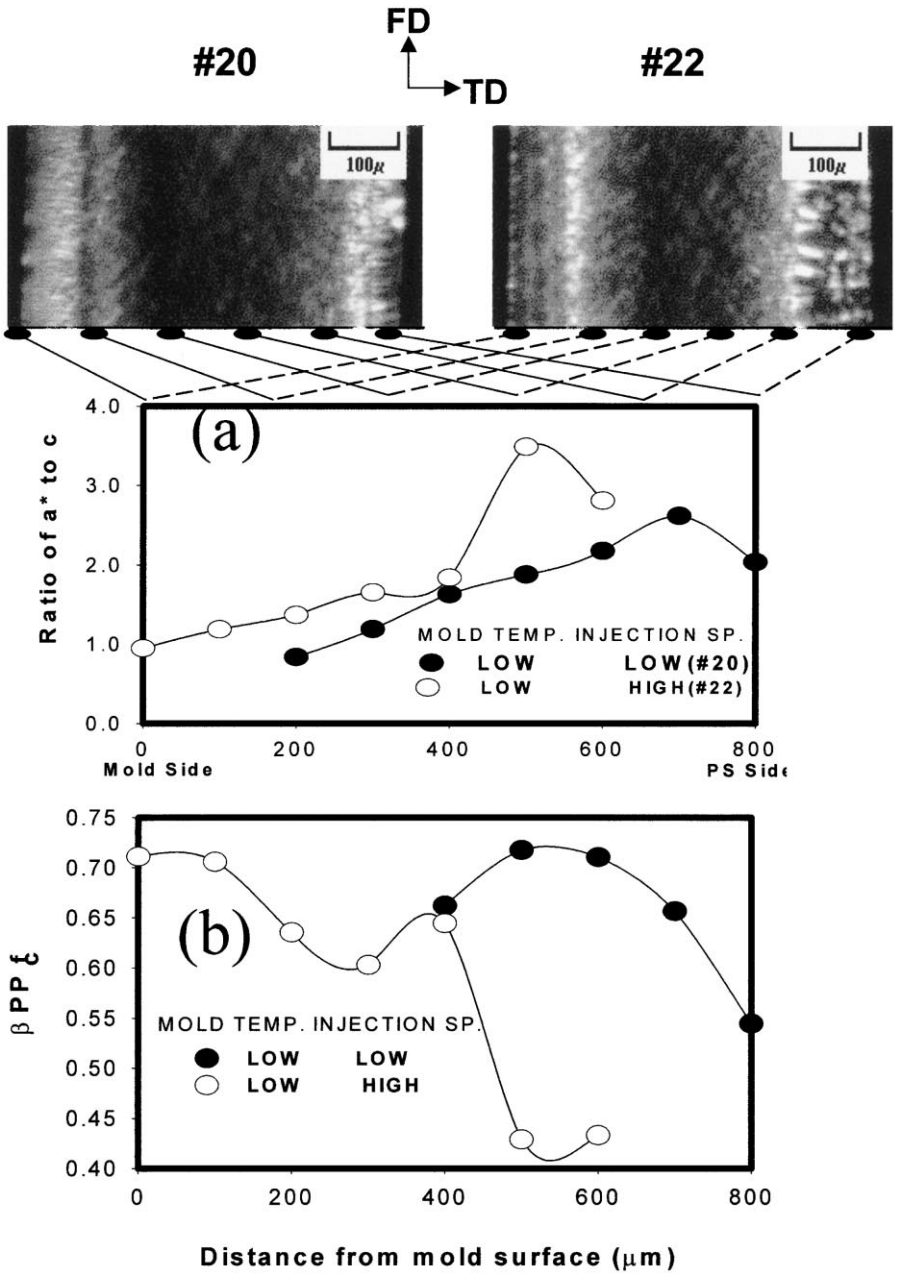

Fig. 18. (a) Ratio of *a*-axis oriented PP to *c*-axis oriented PP, and (b) *c*-axis orientation factors of the β phase.

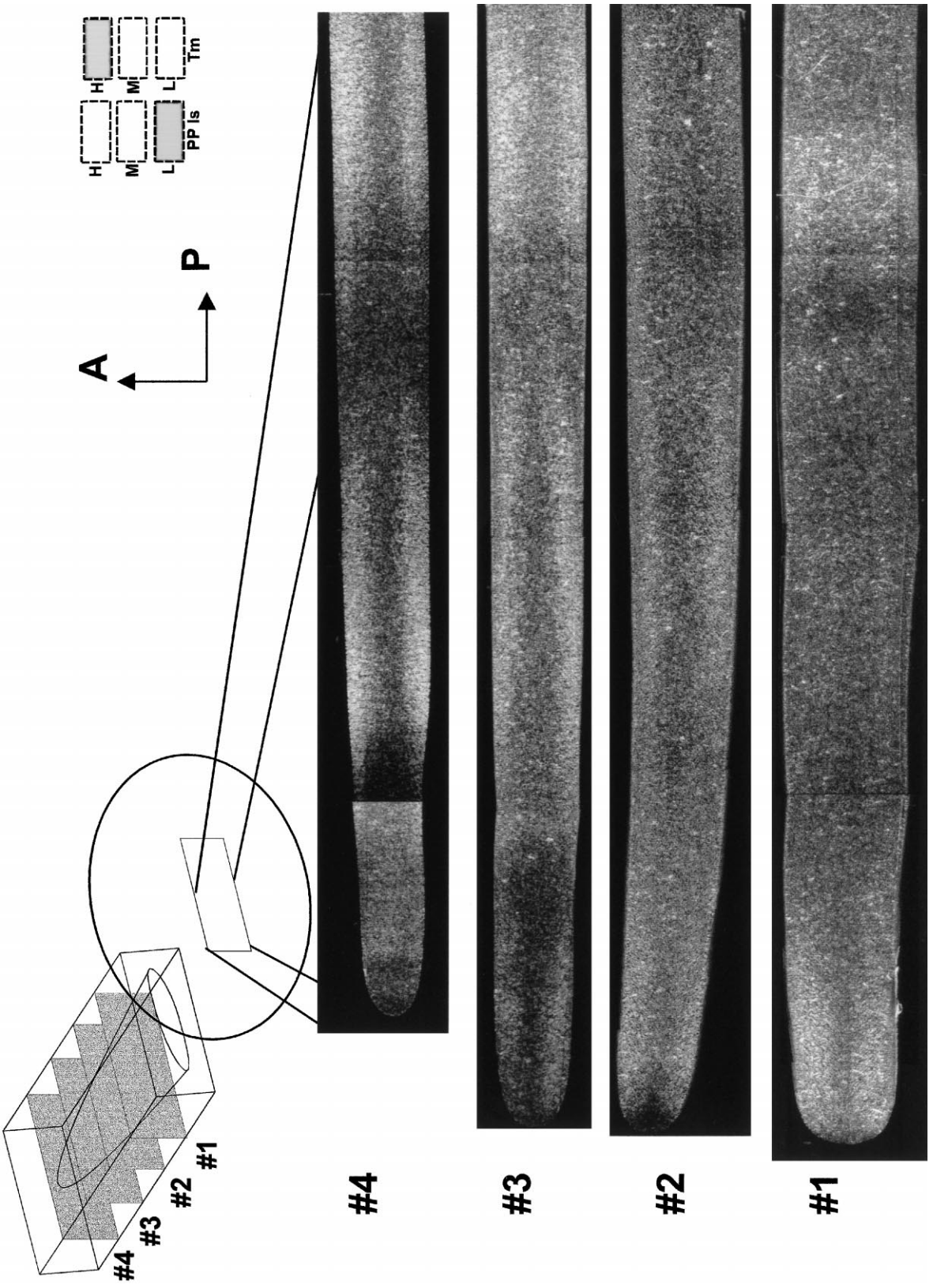

Fig. 19. A-cuts of sample No. 16 with the PP core molded with high mold temperature and low injection speed.

ND–TD plane. Even though two arcs show a broad pattern, their intensity maxima lie almost 45° to the TD–ND direction. Their intensity is contributed to only by the a^*-axis oriented component. Because of the small contribution of the *c*-axis oriented component to skin (040), the comparison of (040) in the skin and core regions shows a significant level of crystallite rotation from skin to core in this region. This result could explain the unusual behavior of the significant tilt observed in this region. The cause of this tilt angle has not yet been identified.

3.6. Structural interpretation

A number of publications shows that polypropylene crystallized under extensional or shear flow conditions exhibits bimodal orientation behavior. One of the orientations is the so-called *c*-axis oriented component and the other is the a^*-axis oriented component. In the *c*-axis oriented component, the *c*-axis is preferentially oriented in the direction of highest deformation. On the other hand, in the a^*-axis oriented component a^* is the reciprocal axis, which makes an angle of 90° to the *b*–*c* crystallographic plane. It is preferentially oriented in the direction of the highest deformation. The (110) plane of monoclinic α shows two different diffraction spots, each corresponding to different orientation modes. The example has already been shown in Fig. 13. Clark and Spruiell proposed the formation of this bimodal orientation by the formation of a secondary crystalline region grown epitaxially in between lamellae of the row structure. They suspected that the epitaxial matching occurs between the 13 Å spacing of the folds of the *c*-axis oriented primary lamellae and the 13 Å spacing between two turns of the 3_1 helix conformation. This is depicted in Fig. 21.

WAXS measurements of Katayama et al. [55] on a melt spin-line indicate that the *c*-axis oriented population crystallizes first and at a higher temperature, and the

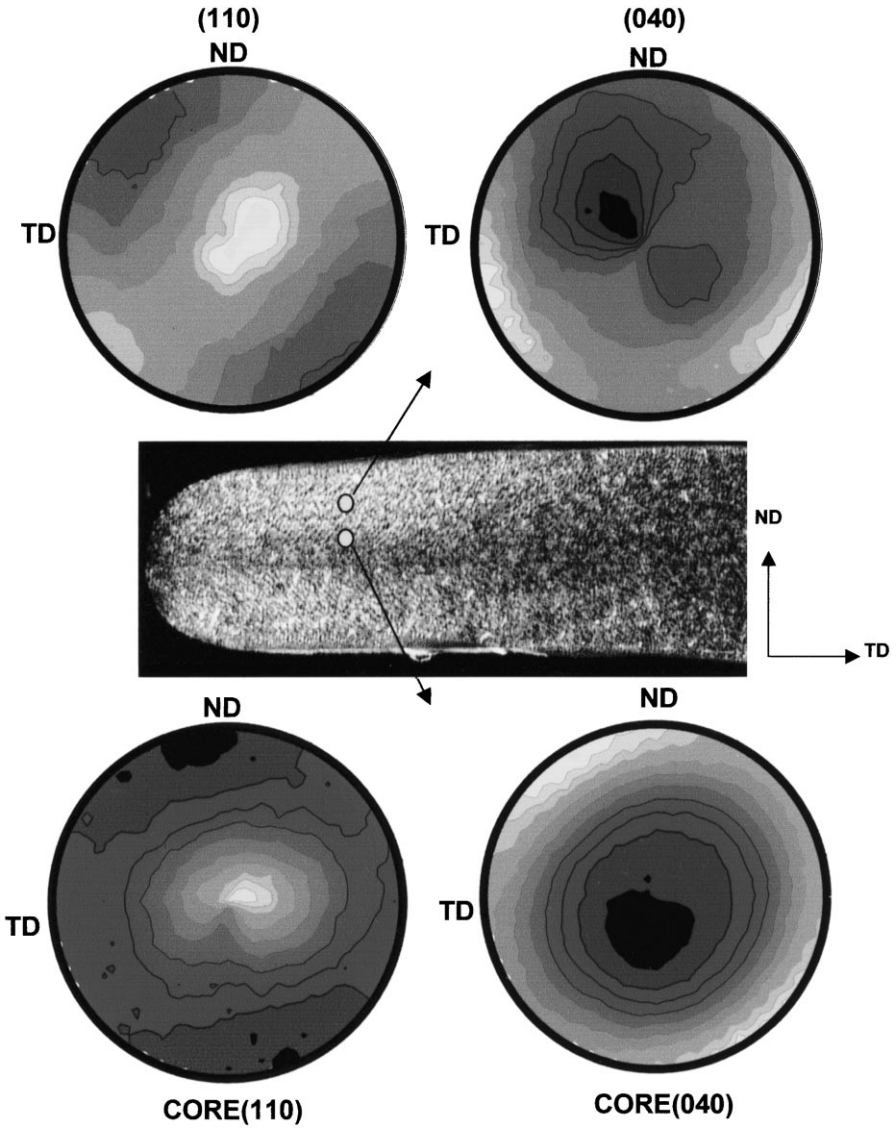

Fig. 20. Isointensity contour plots of pole figures taken at the indicated locations of sample No. 16.

a^*-axis oriented domains crystallize further down the spinline, where the temperature is much lower. Additional evidence comes from their heating experiment, which showed that the a^*-axis oriented crystallites melt earlier than the *c*-axis oriented crystallites [55]. This indicates that the a^*-axis oriented crystallites are smaller and have a lower melting point as a result of their formation at a lower temperature.

More interesting evidence comes from Lovinger's [50] zone solidification experiment. The polypropylene film was crystallized with a temperature gradient of 400°C cm^{-1}. The result shows that the lamellae grow in the direction of the temperature gradient and its growth axis is the a^* direction. This a^*-axis orientation is concluded based on the angular separation between 110 reflections of 36.8° if *a* is radial, or 32.0° if a^* is radial. The (110) diffraction appeared on the meridian, which is the direction of the temperature gradient, while (040) planes are oriented in the direction normal to the temperature gradient. These results clearly demonstrate that under a thermal gradient, polypropylene crystals grow in a^*.

When we examine the WAXS pattern of the normal injection molded samples, in the shear layer we clearly observe the $a^* + c$-axis bimodal orientation. This shear layer is formed during the filling stage and we suspect that *c*-axis oriented crystallites crystallize during the filling stage while a^*-axis oriented crystallites may start to crystallize after the filling stage, and they complete their formation well after the cessation of flow, particularly at the high mold temperature. It is very important to note that a^*-axis oriented crystallites form with their a^*-axis along the flow direction, which is exactly 90° to the steepest temperature gradient. This result clearly indicates that this temperature gradient did not play a role in their directionality and that the epitaxial crystallization mechanism forces the chains in the secondary population to grow at 90° to the highest heat flux vector.

Beyond the boundary of the shear layer, the (110) peaks, corresponding to *c*-axis orientation, greatly decrease while the meridional (110) peak, corresponding a^*-axis orientation, remains relatively high. This result indicates

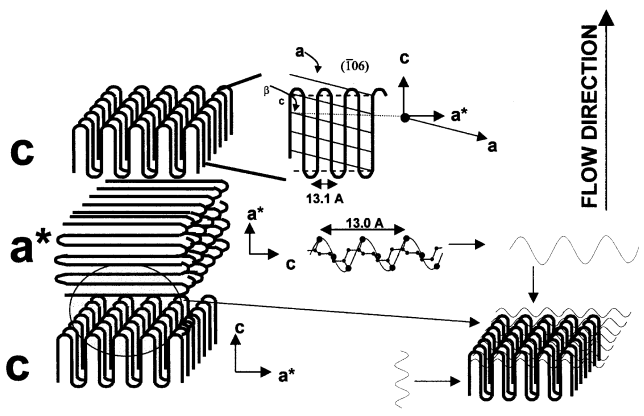

Fig. 21. Structural model for $a^* + c$ crystallization.

that the a^*-axis orientation behavior in FD persists despite the fact that the *c*-axis oriented crystallites have greatly reduced, but that they are not completely absent as indicated by the presence of equatorial intensity in the (110) plane in straight injection molded samples (Fig. 22). We suspect that *c*-axis oriented shish region of the crystallites still persists even towards the interior of the parts.

Hexagonal β is the other type of polypropylene crystal modification observed in processing. Compostella et al. [56] and Ishizuka [57] have reported that slow cooling of polymer melt results in monoclinic modification while rapid cooling results in the hexagonal form. Meille et al. [58] grew the directionally crystallized hexagonal β form utilizing the zone-solidification method. They found that the preferred crystallographic growth direction of β is the *a*-axis which is parallel to the largest heat flux vector (along the steepest temperature gradient). The growth occurs with the twisting caused by the rotation of the lamellae in the *b*–*c* plane. This is shown in Fig. 23. Their X-ray diffraction pattern shows that molecules are oriented with the *c*-axis transverse to the temperature gradient, although the orientation level is not high. The tear-drop-like crystal observed in this figure is of a monoclinic α form. This shape was formed as a result of the growth speed difference between the α and β crystals. The β crystals grow about 20% faster than the α form.

Jinan et al. [59] reported the formation of β modification in the melt spinning process. It was found that at low take-up velocity monoclinic crystals are formed due to relatively higher crystallization temperatures as a result of the slow cooling rate. With increasing take-up velocity, the cooling rate increases and the crystallization temperature decreases. As a result, hexagonal β crystals are formed. Their X-ray patterns show strong (300) diffraction on the equator, which is normal to the temperature gradient direction.

In our co-injection study, skin polypropylene showed fairly high orientation in the transcrystalline layer with the *c*-axis oriented to the flow direction. In sample No. 22 skin polypropylene (which was molded with a high core polystyrene injection speed), two transcrystalline layers were observed resulting in two high β orientation peaks. Even though optical micrographs do not show a bright β phase in the shear region, a strong (300) intensity was observed in the X-ray patterns for this layer that is about 500 μm thick. At the same mold temperature and the same polypropylene injection speed, the straight injection molded sample reveals a fairly thick shear layer that is about 500 μm in thickness. In this shear layer the β peaks were found only in the 200 μm thickness region near the transcrystalline layer (Fig. 22). In skin PP the β phase was observed throughout the thickness. As indicated in the literature, such phases are formed by rapid quenching to 120–130°C in stress-free conditions and in a temperature gradient, or they can be created under flow. It appears that both mechanisms are responsible for the formation of β crystallites.

4. Conclusions

The thickness of core polypropylene decreases along the flow direction while the thickness of skin polypropylene was found to fluctuate, indicating this system is unstable. Injection speed has the greatest effect on the geometry of the core polypropylene. This is primarily caused by its effect on the local kinematics through heat transfer. At slower speeds, the local solid–liquid boundary advances further into the core during injection, as a result, the second polymer spreads more uniformly in the flow direction.

In skin polystyrene the maximum birefringence is observed at intermediate distances between the mold surface and polypropylene surface. The position of maximum value moves towards the mold surface with an increase of injection speed. This change in position is a result of increasing heat generated by the shearing of core polypropylene at a high injection speed.

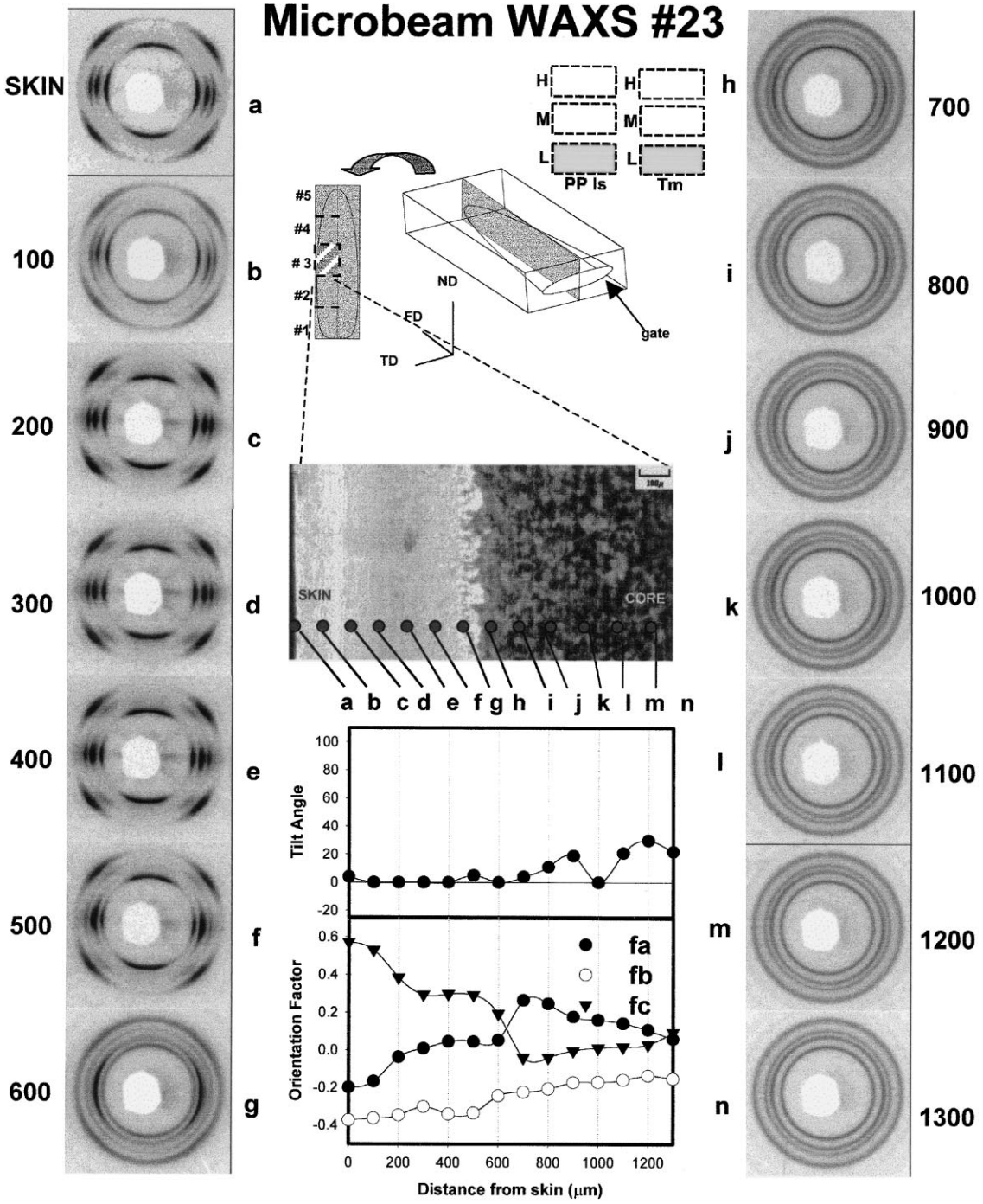

Fig. 22. Microbeam-WAXS patterns, optical photomicrographs and orientation factors for the PP sample molded at low mold temperature with low injection speed.

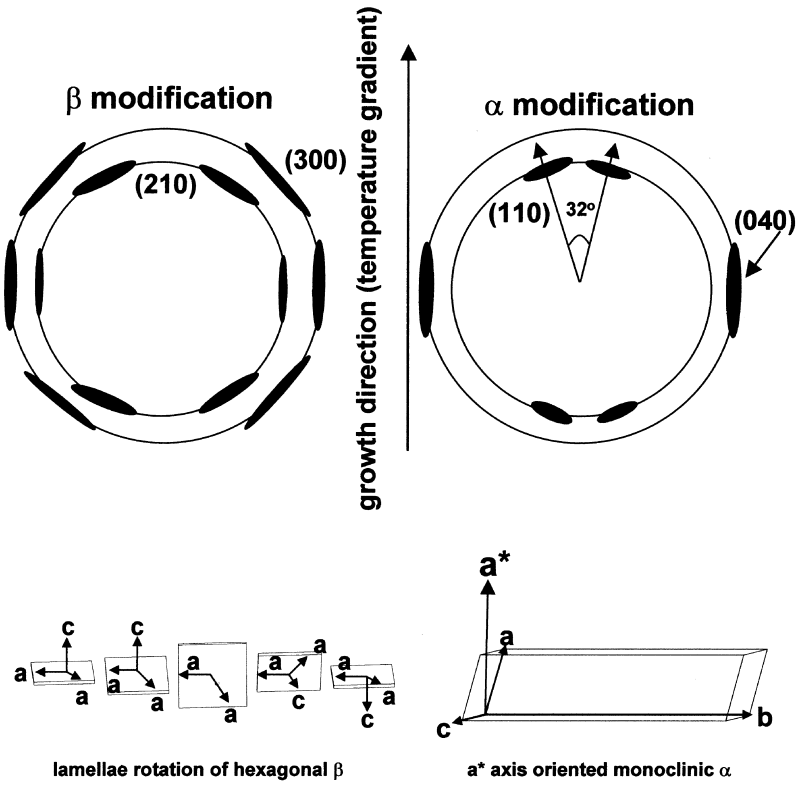

Fig. 23. α and β crystalline orientation developed under a thermal gradient.

Microbeam-WAXS patterns of core polypropylene indicate that although the overall level of the orientation remains low it is still present particularly near the PS/PP interface. In these regions the a^*-axis orientation is generally higher than the *c*-axis orientation. Pole figure WAXS of core PP confirms the $a^* + c$-axis orientation in the skin region and the a^*-axis orientation in the core region. The orientation of the a^*-axis decreases with an increase of injection speed except near the polystyrene surface. We have also observed unusual structural formations in the transverse direction in the core region. The pole figures taken in these regions indicate that they have distinct tilted orientation forming a ''V'' between the two PS/PP interfaces.

When the PP is injected to form the first (skin) layer a high level of *c*-axis orientation observed in the skin polypropylene decreases towards the polystyrene surface while a^*-axis orientation increases. The a^*-orientation crystal population reached its maximum near the polystyrene surface showing that about 75% of the crystalline population is primarily a^*-axis oriented.

Acknowledgements

We would like to thank Dr. S. Toki of the Tonen Corporation for providing the polypropylene for this research.

References

[1] Eckardt H. J Cellular Plast 1987;5:23.
[2] Martin MF, Parsons JL, Albrecht L. Antech 1995;41:4036.
[3] Donovan RC, Rabe KS, Mammel WK, Lord HA. Polym Eng Sci 1975;15 (11):774.
[4] Nagano Y. Japanese patent 48-17492 (to Toyobo) applied for 6/5/69, issued 5/30/73.
[5] White JL, Ufford RC, Dharod KC, Price RL. J Appl Polym Sci 1972;16:1313.
[6] Southern IH, Ballman RL. ACS Polymer Preprints, 1972;13:106; US–Japan Seminar on Polymer Processing and Rheology In: Bogue DC, Yamamoto M, White JL, editors. Applied Polymer Symposia 1978;20:175.
[7] Yu TC, Han CD. J Appl Polym Sci 1983;17:1203. (see also, Han CD. J Appl Polym Sci 1973;17:1289).
[8] Everage EA. Trans Soc Rheol 1973;17:629.
[9] Schrenk WJ, Alfrey T. SPE J 1973;29:38. (also p 43).
[10] Lee BL, White JL. Trans Soc Rheol 1974;18:467.
[11] White JL, Lee BL. Polym Eng Sci 1975;15 (7):481.
[12] Young SS, White JL, Clark ES, Oyanagi Y. Polym Eng Sci 1980;20 (12):798.
[13] Oda K, White JL, Clark ES. Polym Eng Sci 1978;18:25.
[14] Han CD. Rheology in polymer processing. New York: Academic Press, 1976.
[15] Menges G, Liebfried D. Plastverarbeiten 1970;21:S951.
[16] Kantz MR, Newman HD Jr, Stigle FH. J Appl Polym Sci 1972;16:1249.
[17] Menges G, Wubken G, Horn B. Colloid Polym Sci 1976;254:267.
[18] Matsumoto K, Muira I, Hayashida K. Kobunshi Ronbunshu 1979;36:401.
[19] Fujiyama M. Rheoroji Kagaishi 1989;17:5.

[20] Fujiyama M, Wakino T. J Appl Polym Sci 1991;42:2739.
[21] Trotignon JP, Verdu J. J Appl Polym Sci 1987;34:1.
[22] Fujiyama M, Wakino T, Kawasaki Y. J Appl Polym Sci 1988;35:29.
[23] Trotignon JP, Verdu J. J Appl Polym Sci 1990;39:1215.
[24] Fujiyama M. Int Polym Proc 1992;7:84.
[25] Dietz W, White JL, Clark ES. Polym Eng Sci 1978;18:4.
[26] Ulcer Y, Cakmak M, Miao C, Hsiung CM. J Appl Polym Sci 1996;60:669.
[27] Hsiung CM, Cakmak M. J Appl Polym Sci 1993;47:125.
[28] Hsiung CM, Cakmak M. Int Polym Proc 1993;8:255.
[29] Ulcer Y, Cakmak M, Hsiung CM. J Appl Polym Sci 1995;55:1241.
[30] Keuchel K. Master's thesis, University of Akron, OH, 1994.
[31] Kadota M. MS thesis, University of Akron, OH, 1997.
[32] Alexander LE. X-ray diffraction methods in polymer science. New York: Wiley, 1969.
[33] Cakmak M, Hsiung CM, Wang YD. Seikeikougaku ni okeru purasutikku zairyou. Tokyo: Shiguma syuppan, 1997.
[34] Ballman RL, Toor HL. Mod Plastics 1976;38:113.
[35] Jacson GB, Ballman RL. SPE J 1960;16:1147.
[36] Wales JLS, van Leeuwen J, van der Vigh R. Polym Eng Sci 1972;12:153.
[37] Fleissner M. Kolloid Z 1973;251:1006.
[38] Bakerdian Z, Kamal MR. Polym Eng Sci 1977;17:96.
[39] Isayev AI. Injection and compression molding fundamentals. New York: Hanser, 1987.
[40] Isayev AI. Polym Eng Sci 1983;23:271.
[41] Dietz W, White JL. Rheol Acta 1978;17:676.
[42] Isayev AI. J Polym Sci, Phys Ed 1973;11:2123.
[43] Oda K, White JL, Clark ES. Polym Eng Sci 1978;18:1.
[44] Kantz MR, Newman HD Jr, Stigle FH. J Appl Polym Sci 1972;16:1249.
[45] Mencik Z, Fitchmun DR. J Polym Sci, Polym Phys Ed 1973;2:973.
[46] Tan V, Kamal MR. J Appl Polym Sci 1978;22:2341.
[47] Bakerdjian Z, Kamal MR. Polym Eng Sci 1977;17:96.
[48] Clark ES. SPE J 1967;23 (7):46.
[49] Clark ES. Appl Polym Symposia 1973;20:325.
[50] Lovinger AJ, Chua JO, Gryte CC. J Polym Sci, Polym Phys Ed 1977;15:641.
[51] Lovinger AJ. J Polym Sci, Polym Phys Ed 1983;21:97.
[52] Turner-Jones A, Aizlewood ZM, Beckelt DR. Makromol Chem 1964;75:134.
[53] Clark ES, Spruiell JE. Polym Eng Sci 1976;16:176.
[54] Mavridis H, Hrymak AN, Vlachopoulos J. Polym Eng Sci 1986;26 (7):449.
[55] Katayama K, Amano T, Nakamura K. Kolloid ZZ Polym 1968;226:125.
[56] Compostella VM, Coen A, Bertinotti F. Angew Chem 1962;D4:16.
[57] Ishizuka O. Sen-I Gakkaishi 1962;18:198.
[58] Meille SV, Bruckner DR, Lovinger AJ, Padden FJ. Macromol 1994;27:2615.
[59] Jinan C, Kikutani T, Takaku A. J Appl Polym Sci 1989;37:2683.